


A mixture parameterized biologically based dosimetry model to predict body burdens of polycyclic aromatic hydrocarbons in developmental zebrafish toxicity assays

Christian I. Rude¹, Jordan N. Smith^{1,2}, Ricky P. Scott¹, Katherine J. Schultz², Kim A. Anderson¹, Robyn L. Tanguay ^{1,*}

¹Department of Environmental and Molecular Toxicology, Oregon State University, Corvallis, OR 97331, United States

²Biological Sciences Division, Pacific Northwest National Laboratory, Richland, WA 99354, United States

*Corresponding author: 28645, East Highway 34, Corvallis, OR 97333, United States. Email: robyn.tanguay@oregonstate.edu

Abstract

Polycyclic aromatic hydrocarbons (PAHs) are a group of environmental toxicants found ubiquitously as complex mixtures in human-impacted environments. Developmental zebrafish exposures have been used widely to study PAH toxicity, but most studies report nominal exposure concentrations. Nominal exposure concentrations can be unreliable dose metrics due to differences in toxicant bioavailability resulting from disparate exposure methodologies and chemical properties. Toxicokinetic modeling can predict toxicant tissue doses to facilitate comparison between exposures of different chemicals, methodologies, and biological models. We parameterize a biologically based dosimetry model for developmental zebrafish toxicity assays for 9 PAHs. The model was optimized with measurements from media, tissue, and plastic plate walls throughout a static developmental exposure to a mixture of 10 PAHs of high abundance within the Portland Harbor Superfund Site. Plate binding, volatilization, zebrafish permeability, and tissue—media partitioning coefficients vary widely between PAHs. Model predictions accounted for 83% and 54% of 48 hpf body burdens within a factor of 2 resulting from exposures to mixtures and individual PAHs, respectively. Accounting for solubility significantly improves model performance. Competition for active sites in metabolizing enzymes may change biotransformation kinetics between individual PAH and mixture exposures. Area under the curve estimations of concentrations in zebrafish resulted in altered hazard rankings from nominal exposure concentrations. Future work will be oriented to generalizing the model to other PAHs. This PAH dosimetry model improves the interpretability of developmental zebrafish toxicity assays by providing time-resolved body burdens from nominal exposure concentrations.

Keywords: zebrafish; polycyclic aromatic hydrocarbons; dosimetry modeling; toxicokinetics; developmental toxicity

The past 2 decades have witnessed a shift toward large in vitro screens to generate toxicity data to inform decisions of chemical risk in environmental and pharmaceutical applications. This is motivated in part by increased demand for mechanistic hazard data, the greater speed and lower cost of most in vitro tests, and increased societal pressure to reduce, refine, and replace animal testing in chemical decision-making (MacArthur Clark 2018; Beilmann et al. 2019; Thomas et al. 2019; Paul Friedman et al. 2020). Cell-based in vitro models have some disadvantages; namely they have highly specific readouts and can fail to recapitulate or predict complex organ toxicities for which animal models are often better equipped to detect (Beilmann et al. 2019; Weaver and Valentin 2019; Yu et al. 2021; Daley et al. 2023; Juberg et al. 2023). Developmental toxicity assays in *Danio rerio* (zebrafish), fill a crucial niche—combining moderately high throughput in vitro-like capabilities with broad systems-level susceptibility in a vertebrate model (Hill et al. 2005; MacRae and Peterson 2015).

A number of qualities make zebrafish a strong developmental and toxicological model. They develop *ex utero* and near-transparently enabling visualization of organ systems and

morphologic malformations. Embryonic and larval zebrafish fit into a 96-well plate format and consequentially do not require large volumes of chemical for testing. Zebrafish develop most organ systems excluding the gastrointestinal tract within the first 72-h postfertilization (hpf), enabling varying exposure protocols to expose before, during, or after organogenesis (Kimmel et al. 1995; Hill et al. 2005; Garcia et al. 2016). Finally, being vertebrates, they share many organ systems and relevant biological and toxicological processes with humans (Hill et al. 2005; Howe et al. 2013). Due to these strengths and the larger trends in toxicology mentioned above, zebrafish are increasingly used to investigate toxicity, both in mechanistic studies and in large-scale chemical screens such as those conducted in ToxCast (Padilla et al. 2012; Knecht et al. 2013; Geier et al. 2018a; Jarema et al. 2022; Truong et al. 2022).

Toxicity data gathered from developmental zebrafish assays would ideally be used to inform chemical risk assessment. This would require in vitro to in vivo extrapolation in which a dose causing a toxic response in the assay is related to an exposure to an in vivo system of interest through toxicokinetic modeling (Bell et al. 2018). Most large screens of zebrafish toxicity assays report

nominal concentrations in the exposure media. Nominal exposure concentrations can be unreliable surrogates for tissue dose because different chemicals partition between the fish and exposure media to different extents depending on their physiochemical properties (Kühnert et al. 2013; Brox et al. 2016; Geier et al. 2018a). Exhaustively measuring tissue body burdens in developmental exposure assays would greatly decrease throughput and increase cost; however, biologically based kinetic dosimetry models can estimate fish tissue burdens from nominal exposure concentrations.

To date, a number of models have been utilized to describe chemical dose in developmental zebrafish exposures. Siméon et al. (2020) constructed a zebrafish dosimetry model for developmental exposures in commonly used plastic well plates. This model performs well in predicting body burdens of valproic acid analogs after 48 and 96 h of exposure, but overestimates initial body burdens because it assumes instantaneous diffusion between compartments. More recently, models have been developed for perfluoroalkyl substances and 2 for bisphenols (Warner et al. 2022; Billat et al. 2023a, 2023b; Chelcea et al. 2023). Three of these models account for binding to plastic and all of them included limited uptake rates which improves their applicability in early exposure time points. Importantly, no models have been constructed and evaluated for semi-volatile compounds with poor water solubility.

This presents a major dilemma when studying the toxicity of polycyclic aromatic hydrocarbons (PAHs). PAHs are a chemical group characterized by multiple ring structures with aromaticity throughout. They are widely distributed in the environment in complex mixtures (Ravindra et al. 2008; Abdel-Shafy and Mansour 2016; Marques et al. 2016). Owing to their diverse structures, PAHs have multiple modes of toxicity including bioactivation to reactive metabolites, direct interaction with the aryl hydrocarbon receptor, and disruption of potassium channels (Shultz et al. 1999; Genter et al. 2006; Incardona et al. 2006; Siddens et al. 2012; Chepelev et al. 2015; Brette et al. 2017; Garland et al. 2020; Al-Moubarak et al. 2021). A great body of work has been generated utilizing developmental zebrafish toxicity assays to study PAHs, primarily utilizing nominal exposure concentrations (Geier et al. 2018a; Lindberg and Di Giulio 2019; Shankar et al. 2019; Fang et al. 2022). A better understanding of PAH dose in developmental exposure assays, informed by a biologically based kinetic dosimetry model, would greatly improve interpretability and applicability of these studies.

Some work has been done to examine PAH disposition in polystyrene well-plate exposures. PAH binding to polystyrene plate walls is proportional to hydrophobicity and subcooled liquid vapor pressure (Chlebowski et al. 2016; Fischer et al. 2018). Multiple groups have described loss of semi-volatile lipophilic compounds such as phenanthrene within time periods of 24 h in plastic well plate exposures (Schreiber et al. 2008; Kramer et al. 2012; Birch et al. 2019). These phenomenon, along with differences in solubility and tissue-media partitioning, are likely to explain a trend noted by Geier et al. (2018b)—that PAH accumulation in fish tissue increases with octanol-water partitioning coefficients (K_{OW}) for PAHs with $\log K_{OW} < 5.5$, but not for very hydrophobic PAHs. Despite considerable efforts, no toxicokinetic model yet describes developing zebrafish exposures to water-borne PAHs.

This study sets out to understand the exposure dynamics of PAHs within a 96-well plate developmental zebrafish toxicity assay. We build a new biologically based kinetic dosimetry model incorporating plate binding, embryo growth and biotransformation, and

loss of compound from an imperfectly sealed system. The model is parameterized using measured PAH concentrations in the media, plate walls, and embryos tissue at 6 time points over a developmental exposure. We evaluate model performance using PAH body burdens from a previous study, investigate the impact of important model parameters such as solubility and biotransformation, and use it to interpret PAH toxicity data in light of estimated tissue doses.

Materials and methods

Chemical sourcing

Supermix 10 (SM10) was provided by the OSU Chemical Standard Store (OSU CSS) in a 50× solution in DMSO. It consists of the 10 most abundant PAHs measured in the Portland Harbor Superfund site in the molar ratios of their averages measured in sampling campaigns carried out in 2010 and 2015 (Allan et al. 2011; Minick and Anderson 2017; Geier et al. 2018b). All PAHs in SM10 were purchased from Accustandard (New Haven, CT). They are listed in Table 1 along with their molar concentrations in the 50× solution and during exposure. Surrogate standard solution constituents and sources are available in Table S1. Perylene-D12 purchased from Cambridge Isotope Laboratories (Andover, MA) was used as an instrument standard. All PAHs and standards were analytically verified and assessed for purity by the OSU CSS prior to use. Optima-grade ethyl acetate and n-hexanes were purchased from Fisher Chemical (Pittsburgh, PA).

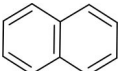
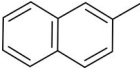
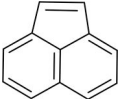
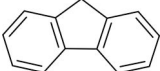
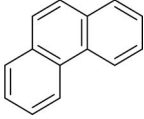
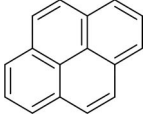
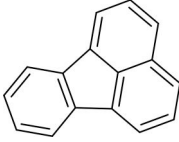
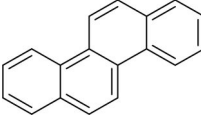
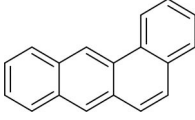
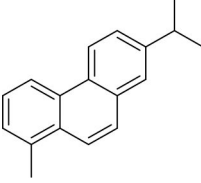
Zebrafish rearing

All embryos utilized for this study were acquired from pathogen-free 5D zebrafish brood stock at the Sinnhuber Aquatic Research Lab under IACUC approval 24-0510. Brood fish are fed twice daily with Gemma Micro (Skretting, Inc. Fontaine Les Vervins, France) and kept on a 14:10 h light:dark cycle. They are maintained in 50-gallon tanks on a recirculating water system supplemented with Instant Ocean salts (Spectrum Brands, Blacksburg, VA, United States) buffered to pH 7.4 with sodium bicarbonate. Fish were spawned at 8 AM, with fertilized eggs collected 1 h later. Quality embryos were selected at 4 hpf, developmentally staged, and dechorionated enzymatically with pronase (Mandrell et al. 2012). At 6 hpf, embryos were robotically plated into 96-well plates in 0.1 ml of embryo media before manual inspection and replacement when necessary. Embryo media consisted of 15 mM NaCl, 0.5 mM KCl, 1.3 mM CaCl_2 , 0.05 mM Na_2HPO_4 , 2.0 MgSO_4 , 4.7 NaCO_3 buffered to 7.2 pH.

Exposures

All exposures were conducted with injections by a D300e Bioprinter (HP, Palo Alto, CA, United States) with light shaking and DMSO as a vehicle solvent. At 8 hpf (75% epiboly), zebrafish embryos were exposed to SM10 at 0.45% of the stock concentration, equivalent to $\sim 39.5 \mu\text{M}$ total PAH. This exposure concentration was the highest exposure concentration resulting in malformations in less than 20% of fish by 120 hpf. This high exposure concentration was chosen to maximize analyte detection and quantification, and is within the range of commonly tested concentrations for PAHs (Geier et al. 2018a, 2018b; Morshead et al. 2025). After injection, plates were sealed with Thermaseal RTS PCR film (Excel Scientific, Victorville, CA, United States) and placed on an orbital shaker set to 300 RPM in a dark incubation room maintained at 28 °C. All plates not utilized in 8.5 hpf measurements were transferred to still, dark incubation boxes at 24 hpf. Plates without embryos termed “fishless plates”

Table 1. Supermix 10 constituents and exposure concentrations.

Chemical	CAS	Structure	Concentration (μM)	
			Whole Mix	Nominal Exposure
Naphthalene	91-20-3		584.9	2.63
2-Methylnaphthalene	91-57-6		174.1	0.78
Acenaphthylene	208-96-8		324.1	1.45
Fluorene	86-73-7		301.0	1.35
Phenanthrene	85-01-8		280.8	1.26
Pyrene	129-00-0		2474	11.1
Fluoranthene	206-44-0		2473	11.1
Chrysene	218-01-9		437.6	1.97
Benz[a]anthracene	56-55-3		438.5	1.97
Retene	483-65-8		1281	5.76

were exposed in parallel to measure PAH binding from the media to the walls of the plate without interference from the developing fish. Method controls were generated using both fish-in and fish-less plates exposed only to DMSO.

Measurements of PAHs in developmental exposures

Samples were sacrificially measured at 8.5, 9, 24, 72, 96, and 120 hpf. The 8.5 hpf and 9 hpf samples were intended to be as close to $t=0$ as possible. Each sample consisted of 36 wells from a

plate, with 2 samples per plate to allow for 25% attrition of developing fish due to SM10 toxicity. For each “fish-in” plate, extracts were acquired from the media, fish tissue, and plate walls as described below. For each “fishless” plate there were only extracts from the media and plate walls. There was 1 replicate at 8.5 hpf and 2 replicates at 9 hpf which were combined for figures into a single point to be able to generate error bars. All other timepoint measurements had at least 3 replicates. Original measurements in tissue, media, and plate walls used for model training in this study are available in [Table S2](#).

Sample collection

Morphologically normal developing zebrafish with media were transferred via glass pipette to a 4ml amber glass vial. The remaining plates were immediately resealed and placed in a freezer at -20°C until extraction. The vials were placed briefly on ice to anesthetize the zebrafish. Media was removed to a separate amber glass vial to comprise the media sample. The fish were rinsed twice with 1 ml of iced media, with each rinse transferred to the media sample vial. After rinsing, fish were transferred to a polypropylene rhino-safe lock tube, flash-frozen in liquid nitrogen, and stored at -20°C until extraction. Media samples were stored in amber vials with Teflon lids at 4°C until extraction.

Tissue extractions

Tissue extractions were adapted from previously verified protocol established by our group (Goodale et al. 2013). Upon removal from the freezer, each sample was spiked with internal standard in ethyl acetate and received $100\mu\text{l}$ of 1 mm glass beads. Samples were thawed over ice for 10 to 15 min. After thawing 250mg Na_2SO_4 and $200\mu\text{l}$ ethyl acetate were added to the samples. The mixtures were vortexed, then homogenized in a bullet blender (Next Advance, NY, United States) at speed 8 for 3 min. An additional $300\mu\text{l}$ of ethyl acetate was aliquoted to each sample. Samples were then vortexed briefly, centrifuged at $1600\times g$ for 10 min at 4°C , and the supernatant was removed to comprise the tissue extract.

Media extractions

For each embryo media sample, a 2.5-ml aliquot was spiked with internal standard solution, and extracted 3 times via liquid-liquid extraction. For each extraction, 0.5 ml of hexane was added, the mixture was vortexed 1 min, and the organic layer was removed to comprise the extract. The 3 sequential extractions were pooled, evaporated under a stream of nitrogen to 0.5 ml, and stored in an amber GC vial until analysis via GCMS/MS.

Plate extractions

For each sample, 12 wells were extracted 3 times with $100\mu\text{l}$ of hexane. Preliminary studies showed less than 5% increased extraction efficiency after 3 extractions (data not shown). The initial extraction was spiked with internal standard in hexane. For each extraction, $100\mu\text{l}$ of hexane was pipetted to the well, sealed with parafilm to decrease hexane evaporation, and recovered after 10 min. Sequential extractions from all 12 wells were pooled to comprise a 3.6-ml plate extract in hexane stored in a 4-ml amber glass vial sealed with a Teflon lid and stored at room temperature until analysis.

GCMS/MS quantification

Extract aliquots of $200\mu\text{l}$ were spiked with instrument standard at $500\text{pg}/\mu\text{l}$ and analyzed on a modified Agilent 7890 B gas chromatograph with an Agilent 700C quadrupole mass spectrometer described previously (Anderson et al. 2015). The CG column used was a $30\text{m}\times 0.25\text{mm}\times 0.15\mu\text{m}$ J&W Scientific Select PAH column (model: CP7462, Agilent, Santa Clara, CA, United States). For each sample, $1\mu\text{l}$ was injected in pulsed splitless mode onto deactivated glass wool in a 4-mm Agilent splitless single-taper liner at 320°C . Samples were loaded with a 35-psi pulse after injection for 0.3 min. Injection purge was accomplished with $25\text{ml}/\text{min}$ flow to the split valve for 0.7 min at 320°C . The oven program is described in Anderson et al. (2015). Helium carrier gas flowed at

$2.0\text{ml}/\text{min}$. The transfer line and source temperatures were held at 320 and 340°C , respectively. The triplepole helium quench gas was set to $2.25\text{ml}/\text{min}$, and nitrogen collision gas at $1.5\text{ml}/\text{min}$. PAHs were identified by mass-to-charge ratio and retention time and quantified on a minimum 6-point calibration curve. Limits of detection were calculated by analyzing replicates of low calibration standards ($n=15$) over 3 days, then multiplying the variance by the 99.5% CI. Limit of quantifications were set at 5 times the limit of detection. Low calibration standards consisted of PAHs at 1 ppb, or the initial concentration in calibrations curves if they were undetected at 1 ppb. A small amount of naphthalene was measured in method controls and was subtracted from sample values.

Measurement QC

Instrument and method performance were verified with calibration verification solutions (CCVs) at the beginning and end of every analytical batch. CCVs were also performed no less than every 10 samples. In total 8 CCVs were analyzed. Recovery of all standards in all CCV runs averaged 103.5% with an average relative percent variance of 8.3%. All calibration verifications were verified at $\pm 30\%$ the true value for $\geq 92.8\%$ of analytes. One post-extraction over-spike was performed for each sample type. The over-spike recovery for fish tissue extract was 102%. For media extract the over-spike recovery was 97.5% and for plate extract, it was 90%. Laboratory blanks included blank solvent and clean media extracts and were run after every calibration verification solution. All laboratory blanks found analyte at or below the limit of quantification. One sample of each sample type was run in duplicate to ensure reproducibility. Duplicate fish tissue analysis had an average relative percent difference of 4.8% and ranged from 0.5% to 20.5%, embryo media displayed an average relative percent difference of 12.7% and ranged from 0.3% to 21.6%, and the plate extract duplicate analysis had an average relative percent difference of 1.5% and ranged from 0.1% to 9.5%. Deuterated internal standards in tissue extracts had an average percent relative deviation (%RPD) of 24% and average recovery of 84%. In media samples, internal standards had a %RPD of 107% and an average recovery of 108%. In plate extracts, internal standards had a %RPD of 13.3% and an average recovery of 98%.

Validation dataset

Measurements from Geier et al. (2018a) were utilized as an external dataset to test model performance, and are referred to throughout the paper as the Geier data. This included reported body burdens from mixture exposures and individual chemical exposures. The mixture used in Geier et al. contains the same chemicals in the same proportions as SM10 except that it utilized acenaphthene instead of acenaphthylene. Mixture and individual chemical exposures were conducted from 6 to 48 hpf. Mixture exposures were conducted at nominal mixture concentrations of 21.9, 11.0, and $5.5\mu\text{M}$ total sum of PAHs. Individual chemical exposures were conducted at nominal exposure concentrations of 25, 11.6, $5.39\mu\text{M}$ for each PAH. All other exposure conditions were conserved between Geier et al. and this study. Tissue extractions followed the same protocols as those used in this study. There are no measurements of PAH from the media or plate walls in the Geier data. Geier data are available in Table S3.

Physiochemical property acquisition

All chemical physicochemical (physchem) properties, unless otherwise stated were obtained from the Comptox Chemical Dashboard Version 2.4.1 (Williams et al. 2017). Experimental

means were used whenever available. When no experimental values were available then the OPERA estimated values provided by the Comptox Chemical Dashboard were utilized (Mansouri et al. 2018). The concentration of retene achieved by passive dosing was used as the water solubility of retene (Incardona et al. 2024). The cheminformatics library RDKit (RDKit Team 2023) was used to calculate solvent-accessible surface area, Van der Waal's surface area, and Van der Waal's volume. Atomic radii for solvent-accessible surface area were calculated using RDKit's Van der Waal's radius method within the periodic table module, whereas for Van der Waal's surface area, radii were calculated using the FreeSASA module. Subcooled liquid vapor pressures were obtained from Epi Suite v4.1 (U.S. EPA 2024). Table S4 contains all physchem properties utilized in this study.

Biologically based zebrafish dosimetry model structure

In order to better understand and quantify chemical dosimetry in the developmental zebrafish system, we developed a biologically based toxicokinetic model of PAH transport. The model consists of 3 compartments including the media, surface of the plastic wells, and zebrafish (Fig. 1). The media compartment consists of solubilized and insoluble fractions of compound. CSL code for the model is available in the Supplementary Material.

Model parameters

Model parameters consisted of physiological values, partition coefficients, and biochemical values that were previously published, experimentally derived, calculated, or optimized. Unless otherwise stated, when describing the model, all concentrations

are in units of μM , all rates are in units of $\text{nmol}\cdot\text{h}^{-1}$, volumes are in ml, and all molar quantities are given in nmoles. Media volumes and surface area of plastic wells were defined by the experimental conditions in 96-well plates and calculated assuming the geometric surface area of a cylinder. The zebrafish volume (ml) and surface area (cm^2) were estimated using a geometric model of an intersecting sphere and cylinder with the sphere representing the yolk and the cylinder representing the embryo body. Derivations for the zebrafish volume and surface area are included in the Supplementary Material and utilize model estimations of the fish's length, abdominal height, and yolk volume from 0 to 120 hpf from Kimmel et al. (1995). Original measurements of fish volumes were determined by the displacement of water volume by 350 embryos at 9, 24, and 49 hpf utilizing the chamber of a Hamilton (NV, United States) 1 ml, model 1001 RN syringe as a graduated cylinder. Each time point was measured for $n=3$ biological replicants. The fish's modeled surface area and volume along with experimentally determined volumes and surface areas from this study and previously published work are displayed in Fig. S1A and B (Guo et al. 2017; Siméon et al. 2020).

Absorption/distribution

In the model, an injected dose of PAH to the media separates instantaneously into dissolved and undissolved fractions. The dissolved fraction is determined by the solubility limit of the compound in 1% DMSO calculated from Equation (1), originally given by Kwon and Kwon (2012).

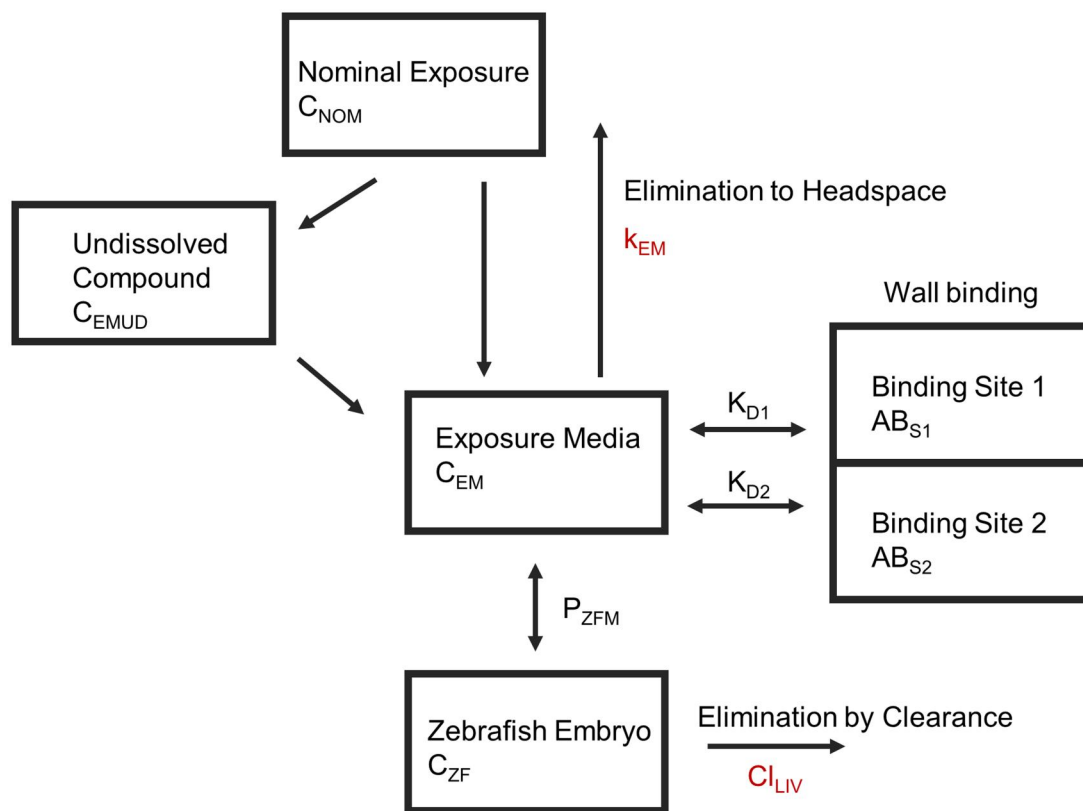


Fig. 1. Structure of the biological-based dosimetry model for developmental zebrafish exposures. Upon addition to the well, the chemical partitions from the media to the plate wall, and zebrafish embryo. Zebrafish clearance, and elimination from the media to the headspace account for loss from the system over time. Zebrafish clearance is scaled to developing liver volume. K_{D1} , K_{D2} , Equilibrium dissociation constants for wall binding; P_{ZF} , Zebrafish—media partition coefficient, diffusion-limited; k_{EM} , Cl_{LIV} , elimination from the system by evaporation to the headspace and liver clearance.

$$\log(\text{Sol}_M) = \log(\text{Sol}_W) + F_{\text{DMSO}} * \sigma_{\text{Sol}}. \quad (1)$$

Sol_M is the solubility in the media (μM), Sol_W is the solubility in water (μM), F_{DMSO} is the fraction of DMSO in the media, and σ_{Sol} ($\log(\mu\text{M})$) is the cosolvency power of DMSO at 1%. Cosolvency power for each PAH is estimated utilizing K_{OW} according to the methods described in Kwon et al. We refer to the dissolved fraction as the PAH in the media that is bioavailable and freely participates in kinetic processes such as elimination to the headspace and partitioning to the fish (C_{EM} , Fig. 1). The undissolved compartment represents a nonaqueous fraction of PAH that is not bioavailable but can dissolve into the aqueous solubilized compartment as the aqueous compartment is depleted through other kinetic processes (binding to plastic, partitioning to the embryo, etc.).

Binding of solubilized PAH in the media to the walls of the plastic wells is modeled with 2 binding sites: A low-affinity high capacity binding site (site 1) and a high-affinity low capacity binding site (site 2). We describe both sites with differential ligand–receptor binding kinetics. The chemical equation for binding of PAH to the well walls at binding site 1 is described in Equation (2), where $[B_1]$ is the concentration (μM) of free binding sites and $[MB_1]$ is the concentration (μM) of bound PAH. The amount of bound PAH (nmoles) and the number of bound sites (MB_1) are equivalent and equal to $[MB_1]$ multiplied by the volume (ml) of media in the well [Equation (3)]. The change in the number of bound sites $\frac{dMB_1}{dt}$ (nmoles $\times h^{-1}$) is equal to the difference between the rate of binding and rate of disassociation [Equation (3)] and the change in the number of unbound sites ($\frac{dB_1}{dt}$) is the reverse [Equation (4)].



$$[MB_1] * V_m = MB_1 \quad (3)$$

$$\frac{dMB_1}{dt} = (k_{\text{on}} * C_{\text{EM}} * [B_1] - k_{\text{off}} * [MB_1]) * V_m \quad (4)$$

$$\frac{dB_1}{dt} = (-k_{\text{on}} * C_{\text{EM}} * [B_1] + k_{\text{off}} * [MB_1]) * V_m. \quad (5)$$

Site 2 and the amount of PAH bound to site 2 are modeled in the same manner as binding site 1. The total amount of a PAH bound to the walls is the sum of binding to both sites.

Absorption of PAH into the zebrafish is modeled with diffusion-limited partitioning. R_{zfm} , the rate of exchange between the media and developing zebrafish (nmoles $\times h^{-1}$), is given by Equation (6), where P_{azf} is the permeability between the media and fish ($\text{cm}\times h^{-1}$), SA_{zf} is the surface area of the zebrafish (cm^2), C_{ZF} is the concentration (μM) in the zebrafish, and P_{zfm} is the partitioning coefficient (unitless) relating the concentrations in the media and zebrafish at thermodynamic equilibrium.

$$R_{\text{zfm}} = P_{\text{azf}} * SA_{\text{zf}} * \left(C_{\text{EM}} - \frac{C_{\text{ZF}}}{P_{\text{zfm}}} \right). \quad (6)$$

We do not include differential partitioning between different compartments of the fish in this model due to limitations in analytical methods and uncertainty in the processes governing transport of chemical within the fish throughout development.

Losses from the system include loss of chemical from the media to the atmosphere by evaporation and elimination of the chemical via the fish's metabolism. PAH elimination by evaporation is modeled as a first-order process with respect to the concentration in the media. Elimination by metabolic biotransformation in the developing zebrafish is modeled using intrinsic clearance (first-order process) with respect to the concentration in the zebrafish scaled by the liver volume. This approach links PAH biotransformation ontogeny to the growth of the liver and assumes a constant activity of enzymes per volume of liver. Since we fit PAH clearance values using PAH concentrations found in the zebrafish embryo, this approach scales total zebrafish clearance, which includes both hepatic and extrahepatic metabolism, to the liver. Scaling to liver volume rather than scaling to body weight offers a distinct initiation time of biotransformation, which is more consistent with observed timing of PAH biotransformation than an immediate onset at conception/exposure (Kühnert et al. 2013; Kühnert et al. 2017; Nawaji et al. 2020). The rate of metabolism, R_{bt} , is given in Equation (7), where R_{bt} is the total rate of biotransformation (nmoles $\times h^{-1}$), Cl_{LIV} is hepatic scaled clearance ($\text{ml}\times h^{-1}\times l_{\text{liver}}^{-1}$), V_{liv} is the volume of the liver (L), and C_{ZF} is the concentration (μM) in the zebrafish.

$$R_{\text{bt}} = Cl_{\text{liv}} * V_{\text{liv}} * C_{\text{ZF}}. \quad (7)$$

The volume of the liver is obtained by multiplying the fractional liver volume by the total volume of the zebrafish.

Liver volume was determined by logistic regression of measured liver volumes determined by confocal microscopy on the Andor BC43 (Oxford Instruments, Abingdon, England) of transgenic zebrafish expressing green fluorescent protein (Gfp) in their liver. The fish contain a construct of Gfp and a 2.8-kb portion of the 5' flanking region of *fabp1a* (Her et al. 2003). Fish were dechorionated at 4 hpf, and imaged at 24, 47, 72, 96, and 120 hpf. Laser intensity and exposure duration were held the same for each image. Liver volumes were measured in imageJ (Fig. S1C). The resulting volumes were divided by the total volume of the fish and fit to the 3-parameter logistic regression model given in Equation (8), where VF_{liv} is the fractional liver volume, $HPF_{50\text{liv}}$ is the developmental time (hpf) at which the liver is half its final fractional body volume, and VF_{maxliv} is the maximum fractional liver volume.

$$VF_{\text{liv}} = \frac{1}{e^{-0.83 * (\text{hpf} - HPF_{50\text{liv}})}} * VF_{\text{maxliv}}. \quad (8)$$

Optimization of parameters

The parameters for each chemical were fit sequentially utilizing measurements from the media, fish tissue, and plate walls. Optimizations minimized the natural logarithm of the sum of squared residuals. Relevant R code for optimizations is included in the Supplementary Material. We began by optimizing for wall binding and elimination to the headspace. Plate exposures without zebrafish revealed 2 kinetic phases of PAH concentrations in the media, evidence of 2 dominant binding sites: A low capacity high-affinity site and a high capacity low-affinity site. As such, we modeled 2 binding sites for all PAHs except chrysene and benz[a]anthracene. Kinetics for chrysene and benz[a]anthracene were monophasic and sufficiently modeled with only one dominant binding site. Low-affinity binding site capacity was set to 1000 nmol $\times \text{cm}^{-2}$ for each compound. High affinity binding site capacity was set equal to the amount of chemical remaining on the well walls at 120 hpf divided by the submerged surface area

of the well. The equilibrium binding constants for both binding site types and the first order rate constant of elimination to the headspace were fit simultaneously utilizing measurements of PAH in the media and well walls in fishless exposures. Measurements at 8.5 and 9 hpf were weighted 3-fold during optimization compared with other values to capture the effect of high early loss from the system. Media samples after 24 hpf lacked adequate acenaphthylene and naphthalene for quantification and media samples after 48 hpf lacked adequate fluorene and phenanthrene for quantification. This prevented simultaneous fitting of both binding sites and elimination for these compounds. Instead, we set the equilibrium binding coefficient for low-capacity sites to $0.0001\ \mu\text{M}$, and fit only high-capacity sites and elimination from the media utilizing all available measurements.

Fitted model parameters pertaining to fish included permeability, the tissue—media partitioning coefficient, and metabolic clearance. Each of these 3 parameters was optimized using tissue measurements from fish-in exposures. We elected not to utilize media concentrations for optimization of permeability and tissue-media partitioning coefficients because concentrations in the embryos are much more sensitive to these parameters than the media due to the tiny volume of the embryos. Tissue—media partitioning was optimized on tissue concentrations from 24 hpf with permeability set to 5. After determining the tissue—media partitioning coefficient, permeability was optimized utilizing tissue measurements from 8.5, 9, and 24 hpf. Finally, metabolic clearance was optimized utilizing all available tissue measurements from 72, 96, and 120 hpf samples. For volatile compounds such as naphthalene, acenaphthylene, fluorene, and phenanthrene, clearance rates were fit with very small tissue concentrations. Smaller apparent clearances for these compounds corroborate previously reported findings (Nichols et al. 2013, 2018), but may be artificially low due to fitting with tissue concentrations near analytical limits.

Optimization of models with shifted metabolic onset was performed using a grid optimization that solved for clearance and tissue—media partitioning coefficients under different combinations of permeability and metabolic onset times. Permeability values included 0.1, 0.3, 0.5, 1, 3, 5, $10\text{ cm}\times\text{h}^{-1}$. Metabolic onset time was altered by shifting the 50% fractional liver volume time from 97.2 hpf to 84, 72, and 60 hpf, thereby breaking the ontology between biotransformation rates and liver volume. Clearance and tissue—media partitioning coefficients were optimized simultaneously under each combination of metabolic growth times and permeability utilizing tissue concentrations at 24, 48, 72, 96, and 120 hpf. Tissue measurements at 24 hpf were weighted at 3 times the standard measurement, and tissue measurements at 48 hpf were weighted at 1.5 times from all the other points.

Sensitivity analysis

Local sensitivity analysis of the area under the curve dose (AUC) ($\mu\text{M}\times\text{h}$) was conducted for fish-specific parameters and chemical-specific parameters for each of the parameterized chemicals in SM10. For each compound, the analysis was conducted utilizing a hypothetical single static exposure from 8 to 120 hpf with a starting nominal media concentration of $5\ \mu\text{M}$. This concentration was chosen because it is within the apparent solubility for all compounds in SM10 excluding benz[a]anthracene and chrysene and most PAHs do not cause developmental malformations in zebrafish below this concentration. The local sensitivity coefficient was calculated as the relative change in

the AUC divided by the relative change of the parameter. For each sensitivity test, the relative change in parameter was 20%.

Model performance

Model performance was assessed utilizing the mean square error of the \log_{10} values (MSE), the log-likelihood ($\ln(\hat{L})$), and Akaike Information Criterion (AIC). We assume measured values can be approximated by a normal distribution, in this way the log-likelihood is defined in Equation (9), where n is the number of data points and RSS is the residual square error.

$$\ln(\hat{L}) = -\frac{n}{2} \times [\ln(2\pi) + \ln(\text{RSS}) - \ln(n) - 1]. \quad (9)$$

AIC was calculated utilizing Equation (10), where k is the number of estimated parameters within a model (Akaike 1998).

$$\text{AIC} = 2k - 2\ln(\hat{L}). \quad (10)$$

Software utilized

All statistics and analysis, unless otherwise stated were conducted in R version 4.3.2 in RStudio (R Core Team 2023, 2024). All figures were generated in ggplot2 (Wickham 2016). DRC was utilized for loglogistic modeling (Ritz et al. 2015). Dosimetry models were built in Magnolia Version 1.3.9 (Magnolia Sciences, LLC, Orlando, FL, United States) and implemented in R using the RMagnolia package (Magnolia Sciences). When optimizing the model for multiple parameters simultaneously, the function `optim` was used with the limited memory, quasi Newtonian, L-BFGS-M method, to minimize the residual sum of squares of log residuals (Byrd et al. 1995). When solving for single parameters, the function `optimize` was used. RDkit was implemented in Python (Python Software Foundation, www.python.org).

Results

Model fits and measurements

We evaluated PAH mass balance from 96-well plate exposures as determined by summed quantities of PAHs measured in the media, plate walls, and zebrafish at each time point for both fish-in and fishless exposures (Fig. S2A and B). In general, in both fish-in and fishless exposures, more volatile compounds display higher loss from the system, whereas more hydrophobic compounds bind to plate walls in greater abundance. Volatile compounds such as naphthalene, 2-methylnaphthalene, and acenaphthylene, were depleted by more than 75% within the first 30 min of exposures in both fish-in and fishless exposures. For all compounds except benz[a]anthracene and chrysene, preliminary extractions of adhesive plate seals at 16 h postexposure contained 10% to 30% of the mass balance, suggesting volatilization followed by partitioning to plate seals is the main driver of loss for volatile PAHs (data not shown). Compounds such as pyrene, fluoranthene, phenanthrene, and retene, showed more gradual, but still significant loss in both fish and fishless exposures. They were depleted by 25% to 50% within the first 30 min, and between 87% and 98% in 120 hpf measurements. In fish-in and fishless exposures, benz[a]anthracene and chrysene primarily partitioned to the wall. Neither of them displayed significant loss of compound in fishless exposures after the first 30 min; both were depleted some during fish-in exposures.

After parameterizing the model for all SM10 compounds except for 2-methylnaphthalene, the compounds were classified

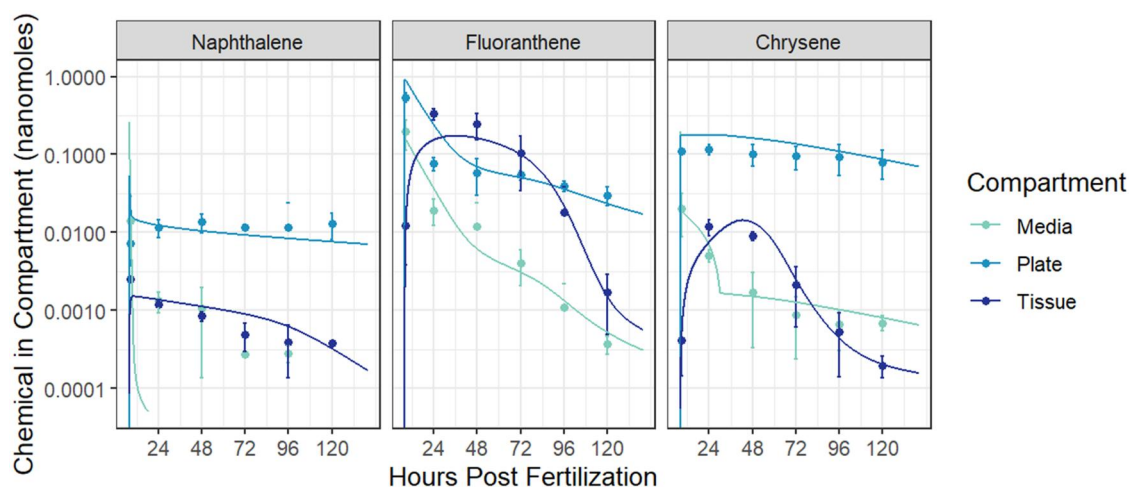


Fig. 2. Example compounds demonstrating 3 patterns of PAH distribution to fish tissue (dark blue), media (light blue), and plate walls (blue) resulting from static waterborne exposure of dechorionated zebrafish embryos to SM10 from 8 to 120 hpf. Naphthalene represents the volatile group, fluoranthene represents the bioavailable group, and chrysene represents the hydrophobic group. Model predictions are depicted by solid lines. Mean GC-MS measurements are depicted by points with 95% CIs from 3 to 4 biological replicates consisting of 36 plate wells. When no error bar is present, only one measurement was above the LOD. When no point is present, no chemical was measured above the LOD.

into 3 groups based on their distribution among the embryos, media, and plate wall: A volatile group, a bioavailable group, and a hydrophobic group (Fig. 2). The volatile group includes acenaphthylene and fluorene. These compounds leave rapidly from the system, adhere to the plate only at low capacity high affinity binding sites (site 2), and distribute minimally to the zebrafish embryo. They achieve total tissue doses equivalent to less than 5% of the initial added compound, and by model estimations achieve their maximum dose within 2 to 4 h of exposure. Fluoranthene is part of the bioavailable group which also includes phenanthrene and pyrene. For chemicals in this group, the zebrafish tissue compartment contains the highest fraction of the added PAH at some point during the exposure. They are less volatile, utilize both types of binding sites, and achieve internal doses between 7% and 20% of the initial added chemical mass. They achieve their maximum doses later, between 8 and 37 h after exposure. Fluoranthene and pyrene are significantly more bioavailable achieving internalized doses of 15% and 20% compared with just 7% for phenanthrene. Retene, chrysene, and benz[a]anthracene are part of the hydrophobic group. These are chemicals for which C_{nom} was well above their solubility limit. They are characterized by low loss from the system and large chemical loads within the plate walls. Plate walls remain the dominant compartment by chemical mass throughout the exposure. Despite this, they still achieve significant body burdens equivalent to 6%, 7%, and 15% of the mass balance for retene, chrysene, and benz[a]anthracene, respectively. Model fits and measurements are available for all 9 parameterized chemicals in Fig. S3. Chemical-specific parameter values are available in Table S5.

Sensitivity analysis

The PAH concentration in zebrafish AUC ($h \times \mu M$) was sensitive to the biotic parameters of embryo surface area and volume for all chemicals, and was sensitive to the onset of liver growth for hydrophobic compounds (Fig. 3A, Fig. S4). Increases in surface area positively impacted AUC for all chemicals due to the direct input of surface area on the rate of chemical transfer between the fish and media [Equation (6)]. Increases in fish volume result in decreases in the AUC embryo dose. Because metabolic capacity is scaled by liver volume in this model, a delay in liver

growth results in an increased AUC; however, this increase is most relevant when the loss due to volatilization is small. The sensitivity to liver growth time is best viewed by scaling the sensitivity to the concentration within the fish tissue (Fig. 3C, Fig. S6) because sensitivity to AUC is less impactful by later timepoints due to very small concentrations within the fish. Viewed in this manner, the onset of liver growth time meaningfully impacts the tissue AUC for benz[a]anthracene and chrysene, but is less influential for other compounds in SM10 (Fig. S7).

PAH permeability and the zebrafish-media partitioning coefficient were important in determining PAH concentration in zebrafish AUC for all PAHs, whereas sensitivity to other parameters such as solubility, plate binding affinity, metabolic clearance, and the rate of elimination from the media varied highly among chemicals (Fig. 3B, Fig. S5). With increasing volatility, AUC is increasingly sensitive to the rate of elimination from the media and decreasingly sensitive to clearance rates. Conversely, with increasing molecular size and hydrophobicity, solubility and clearance become increasingly influential parameters. Chemical-specific embryo permeability was strongly influential on the AUC dose for all chemicals and mirrored that of surface area (Figs S4 and S8). The AUC for volatile compounds such as naphthalene, acenaphthylene, fluorene, and phenanthrene was also sensitive to the rate of elimination from the media but not plate binding affinity or metabolic clearance. For less volatile compounds such as fluoranthene, pyrene, and retene, plate binding affinity and elimination from the media had similar magnitudes of effect on AUC. For chrysene and benz[a]anthracene, AUC was negligibly sensitive to plate binding and elimination from the media. Instead, solubility was the most influential parameter, likely because it limited the bioavailability of these compounds. Permeability, embryo-media partitioning, and clearance were also influential parameters for benz[a]anthracene and chrysene. For all compounds, the embryo-media partitioning coefficient was the third or fourth most influential parameter to AUC.

Model performance

The zebrafish dosimetry model accurately predicts 48 hpf body burdens in both mixture exposures and individual PAH exposures from the Geier dataset (Fig. 4A and B). It predicted 83% (20/24) of

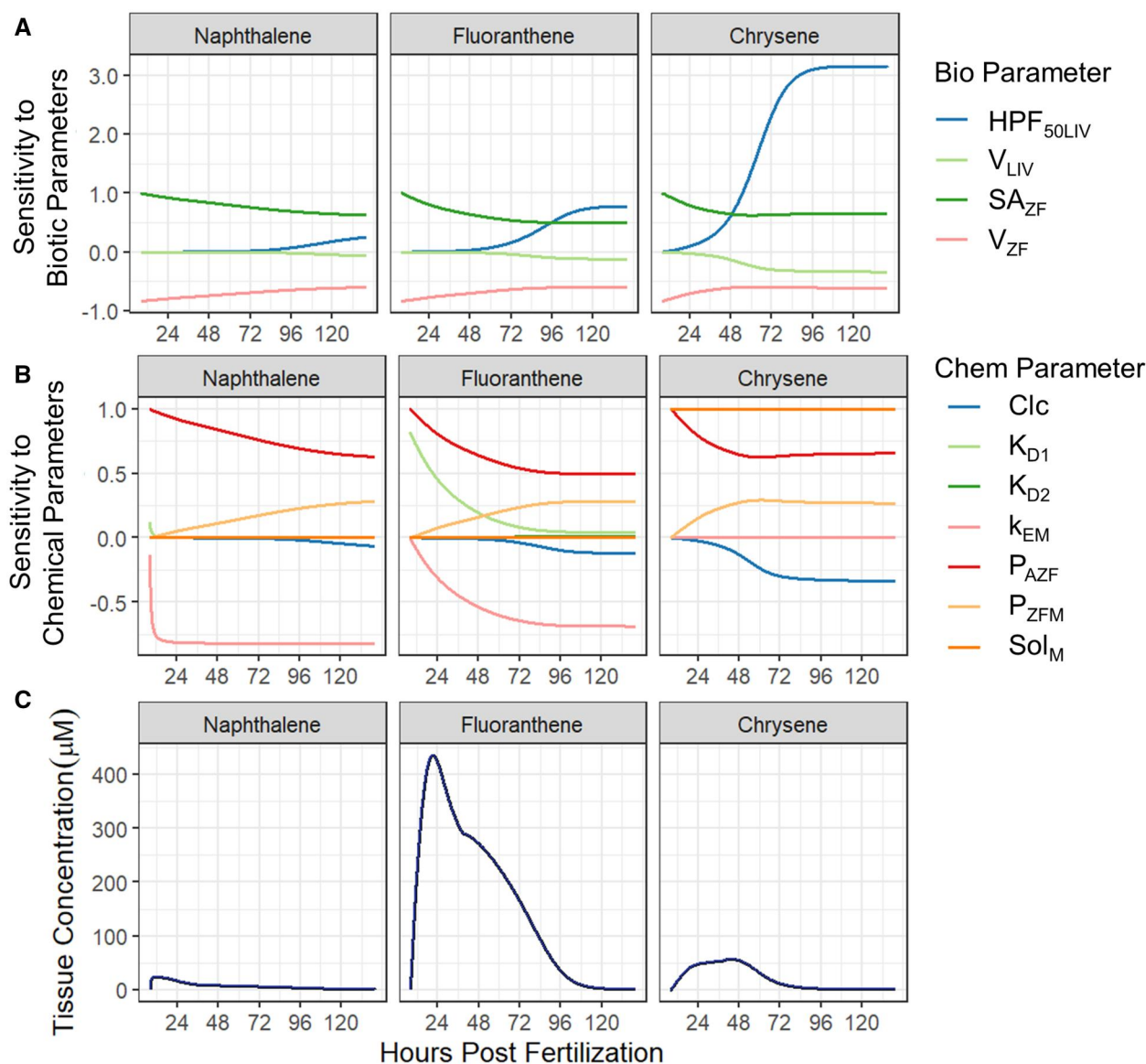


Fig. 3. Sensitivity of the AUC (μMxh) tissue dose to A) biological parameters and B) physchem parameters during simulated exposure of developing zebrafish embryos to naphthalene, fluoranthene, and chrysene from 8 to 120 hpf at nominal concentrations of 5 μM. C) The modeled tissue concentration throughout the exposure. HPF_{50LIV}, 50% liver growth time; V_{LIV}, the liver volume; SA_{ZF}, zebrafish surface area; V_{ZF}, zebrafish liver volume; Clc, zebrafish clearance; K_{D1}, binding site 1 equilibrium concentration; K_{D2}, binding site 2 equilibrium concentration; k_{EM}, first-order rate of volatilization; P_{AZF}, permeability of the zebrafish; P_{ZFM}, zebrafish—media partitioning coefficient; Sol_M, media solubility of compound.

48 hpf body burdens of mixture exposures within a factor of 2 and 92% (22/24) within a factor of 5. For individual chemical exposures at high concentrations, the model predicted 54% (13/24) of body burdens within a factor of 2 and 87% (21/24) of body burdens within a factor of 5. Most of the error in body burden prediction for the dosimetry model arises from predictions of chrysene, benz[a]anthracene, and retene which together account for 85% of the residual squared error in individual PAH exposures. Larger errors of body burden predictions for these PAHs in individual PAH exposures may result due to their exposures being well above their solubility limits in individual PAH exposures or due to mixture effects on clearance rates resulting from inhibition by other PAHs.

Effect of solubility and AUC dose and model performance

We evaluated the effect of solubility on model performance by parameterizing a solubility-agnostic model and comparing model

performance to the original model. The original model is referred to as the solubility model throughout this section. We refer to the data generated in this study that measured PAH concentrations in the tissue, media, and plate walls as training data. Goodness of fit to the training data was evaluated by comparing the MSE of the 2 models for the amount of PAH in embryo tissue and the MSE for the amount of PAH in all 3 compartments (Fig. 5A). When examining the MSE for model fits to PAH in the tissue from training data, the solubility model performed better for every constituent of SM10 exposed at a nominal exposure concentration above its solubility. This included pyrene, fluoranthene, retene, chrysene, and benz[a]anthracene. When examining the MSE for all compartments, only chrysene and benz[a]anthracene, the 2 compounds that exceeded their solubility limits to the greatest extent, had better performance in the solubility model. The MSE for all compartments for retene, fluoranthene, and pyrene, were comparable between the solubility and solubility

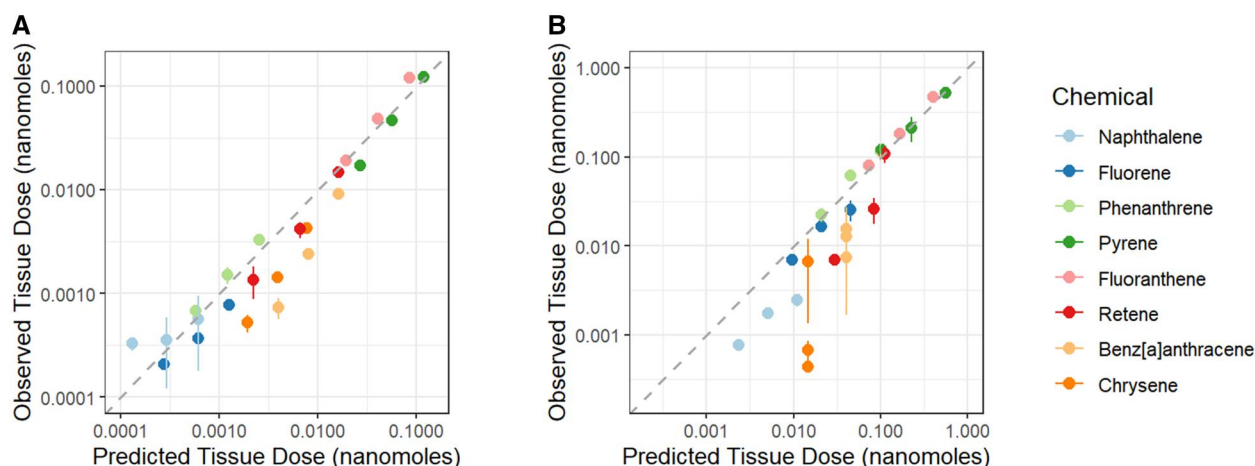


Fig. 4. Predictions of body burdens from nominal exposure concentrations reported in Geier et al. (2018b) for A) mixture exposures and B) single chemical exposures. Error bars depict 95% CIs or measured body burdens resulting from exposures to PAH in 96-well plates from 6 to 48 hpf. The dotted gray line represents perfect estimations.

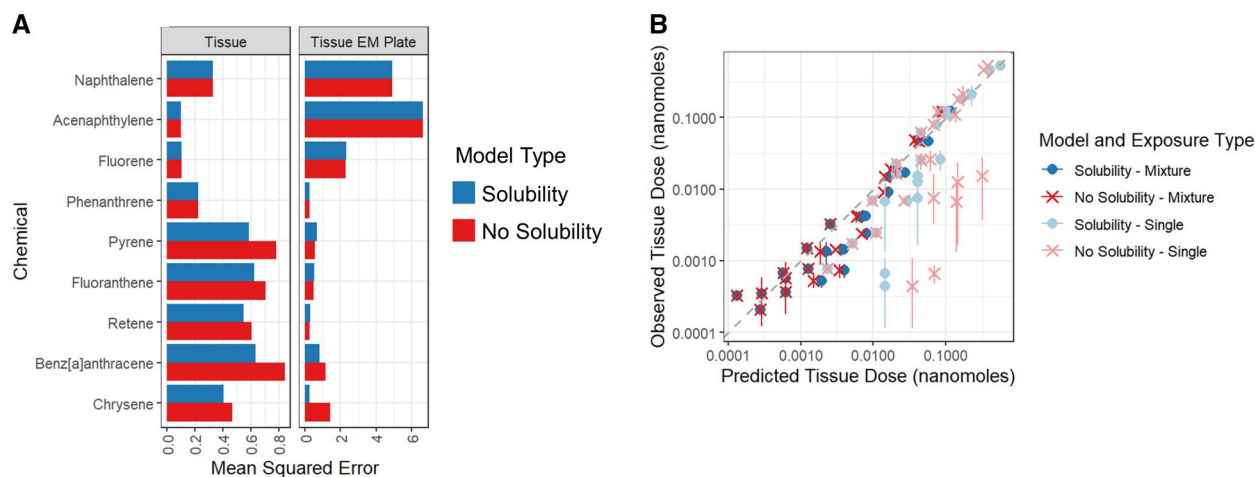


Fig. 5. A) The MSE \log_{10} values of model outputs for chemical in the tissue alone and chemical in tissue, embryo media, and plate wall for the solubility model in blue and solubility agnostic model in red for each measured PAH. B) Model estimates and measured body burdens for PAHs from Geier et al. Solubility model estimates are blue circles and solubility agnostic model estimates are red X's. Mixture exposure values are displayed in darker tones, whereas individual chemical exposures are displayed in lighter tones. Error bars include the 95% CI for each experimental value as estimated from 3 biological replicates.

Table 2. AIC for solubility and solubility agnostic models predicting body burdens from Geier et al. (2018b).

Model	Exposure method	AIC
Solubility	Single	180.7
No Solubility	Single	222.7
Solubility	Mixture	84.4
No Solubility	Mixture	55.1
Solubility	Single and Mixture	196.8
No Solubility	Single and Mixture	229.1

agnostic model. No difference in model performance was observed for any of the compartments for compounds exposed below their nominal exposure concentrations to generate training data (Fig. 5A).

The predictive performance of the 2 models was also evaluated by computing the AIC of each model's predictions of 48 hpf body burden from the Geier dataset (Fig. 5B, Table 2). Again, the solubility model performs better when nominal exposure concentrations exceed solubility limits. The solubility model predicts

PAH body burdens from individual chemical exposures in the Geier dataset closer to measured values than the solubility agnostic model, but performs nearly equivalently in predicting body burdens resulting from mixture exposures from the Geier dataset (Fig. 5B). Consequentially, the solubility model has lower AIC than the solubility agnostic model for the individual exposure data from Geier et al., but higher AIC than the agnostic model for mixture exposures. This is likely because the individual chemical exposures from the Geier dataset tended to exceed their predicted solubility limits more than the mixture experiments. When including all Geier data in calculating the AIC, the solubility model performs slightly better than the agnostic model. This, along with the frequency at which PAHs are exposed above their solubility limits in routine testing, leads us to conclude that accounting for solubility adds value in developmental zebrafish dosimetry modeling.

The nominal concentration at which media solubility limited the AUC dose of chemical in fish varied greatly among chemicals, but was higher for volatile compounds than nonvolatile compounds. To examine at what nominal exposure concentrations the

media solubility of chemical limited AUC tissue dose, we calculated sensitivity coefficients for media solubility and nominal concentrations for simulated exposures from 0.01 \times to 1000 \times the solubility limit for each parameterized PAH. The sensitivity coefficient can be interpreted as the fractional effect to the AUC dose of a change in the parameter of interest; a sensitivity coefficient of 0.5 indicates that under local conditions, a relative change in the solubility limit of 0.2 resulted in a relative change in the AUC dose of 0.1. The sensitivity coefficient of solubility remained near zero until nominal exposure concentrations were far above expected solubilities for all PAHs (Fig. S10A). For naphthalene, the most volatile compound, the sensitivity coefficient of solubility reached 0.5 at ~ 99 mM about 386 \times its expected solubility. For benz[a]anthracene, a nonvolatile compound, this occurred at 2.89 μ M, about 41 \times its solubility limit. The Spearman correlation between sensitivity to nominal exposure concentration and volatility was 0.91 (P -value < 0.05). As expected, the sensitivity coefficient of nominal concentration followed an inverse relationship to that of the solubility limit (Fig. S10B). These

results indicate that while exceeding the solubility limit in exposures introduces considerable uncertainty in the derived dose-response relationship, the solubility limit does not immediately limit the dose of PAH taken up by the embryo.

Investigation into the onset of biotransformation

We tested the ontological link between the rate of biotransformation and liver volume in by incrementally shifting biotransformation onset earlier than liver growth and comparing the resulting fits to training data. Metabolic onset was shifted by changing HPF_{50liv} from 97.2 hpf to 84, 72, and 60 hpf (Fig. 6). In this analysis, we refer to HPF_{50liv}, the 50% fractional liver growth time, as the metabolic growth time because it no longer reflects measured liver volumes. Optimizations of clearance and zebrafish-media partitioning were performed over a grid of static permeabilities and metabolic growth times to reduce dimensionality.

No singular combination of metabolic growth time and permeability value performed the best for every PAHs included in

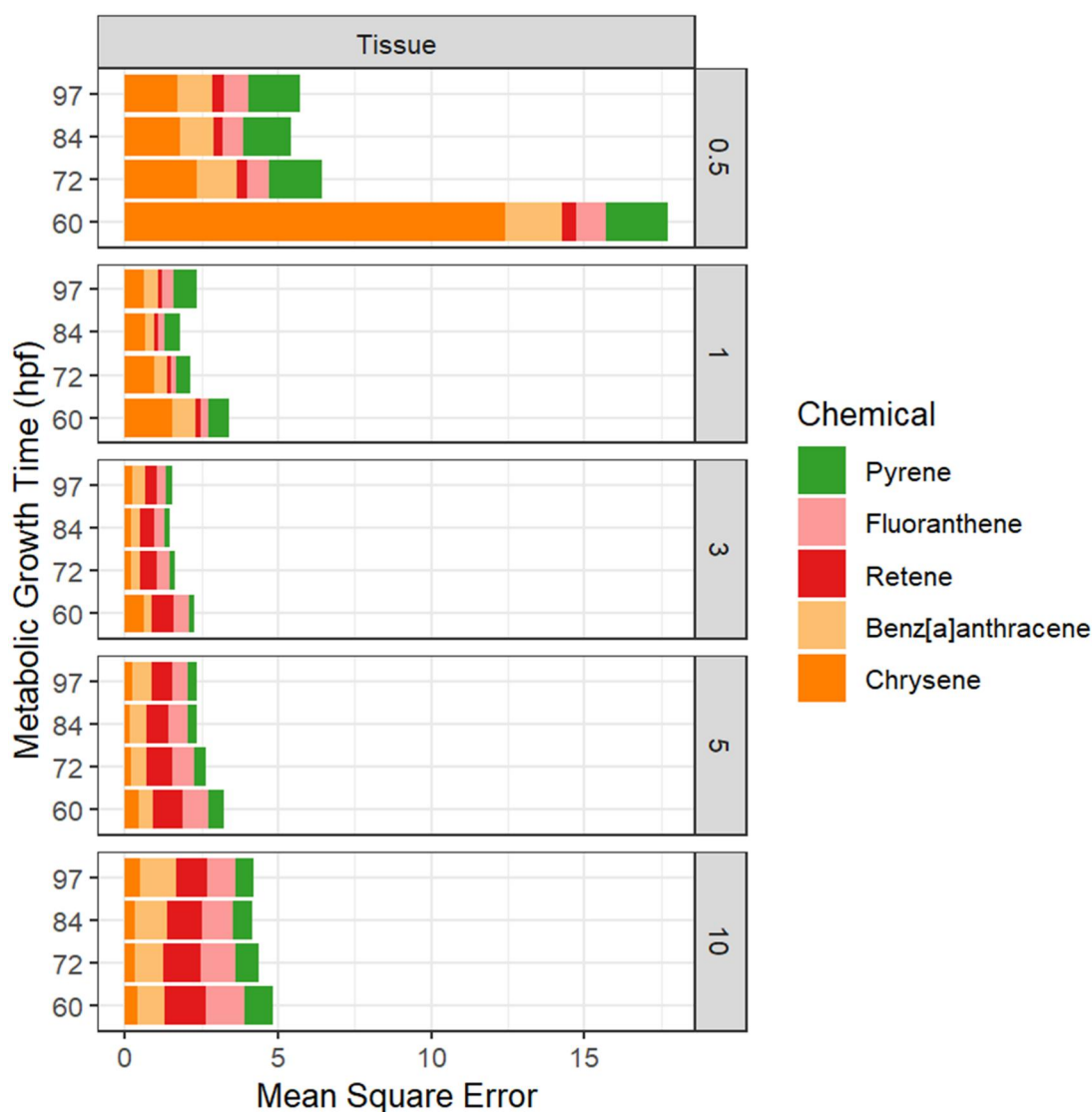


Fig. 6. The MSE \log_{10} values of tissue burdens for pyrene, fluoranthene, chrysene, benz[a]anthracene, and retene with regard to training data. Metabolic growth time refers to the time at which clearance is scaled to 50% of its maximum fractional embryo volume and facet values refer to zebrafish permeabilities (0.5, 1, 3, 5, 10). The model was parameterized for fish—media partitioning coefficients and scaled clearance for each combination of zebrafish permeability and metabolic growth time. Optimizations were performed using measurements from the fish tissue at hpf = 24, 48, 72, 96, and 120.

the analysis. The 2 condition sets with the lowest cumulative errors have metabolic growth times of 84 and 96 hpf and a zebrafish permeability $3 \text{ cm} \times \text{h}^{-1}$. The model with metabolic growth time at 84 hpf has the lowest error ($\Sigma\text{MSE}_{84}=1.47$, $\Sigma\text{MSE}_{96}=1.57$), but with a relative likelihood of 0.36, there is not significant evidence to firmly support either metabolic growth time. It appears then, that early variation in clearance capacity occurring from extrahepatic metabolism can be adequately accounted for in the apparent clearance we obtain by scaling to liver volume.

Comparison to PhysChem properties

Generalization of the model to other PAHs will require estimation of model parameters from physchem properties. Chemical-specific model parameters were tested for linear or log-linear correlations to physchem properties to access the prospects of future generalizability to other PAHs and access if model parameters truly described their intended processes. Significant log-linear relationships existed between plate wall binding affinity and K_{OW} (Fig. 7A), elimination from the media and K_H (Fig. 7B), and hepatic clearance and K_{OW} (Fig. 7C). There was no significant log-linear correlation between intrinsic clearance and the first order rates of clearance predicted by OPERA or EPI Suite's BCFBAF (Fig. S11A and B). The relationship between rates of biotransformation and K_{OW} has been noted in other studies (Arnot et al. 2008; Franco et al. 2022). PAH metabolism by Cyp1a is largely influenced by Vander walls forces within the Cyp1a active site and proximity of the substrate to the heme iron (Chen et al. 2021). For PAHs metabolized by Cyp1a in zebrafish, higher

clearance rates for higher K_{OW} PAHs likely result from larger compounds fitting more favorably within the Cyp1A active site, rather than a direct relationship between K_{OW} and biotransformation (Chen et al. 2021). The above-noted relationships in parameters for plate binding, elimination from the media, and clearance imply that they characterize their intended processes.

Logarithmic values of permeability for each PAH scaled most positively with measurements of molecular size such as Van der Waal's volume, Van der Wall's surface area, and solvent available surface area (Fig. 7D, Fig. S12). The observed relationship for permeability is nonsensical and indicates permeability may be unduly influence by bioavailability for hydrophobic compounds and rapid loss for volatile compounds. Similarly, confidence in fitted zebrafish—media partitioning coefficients is called into questions by its lack of correlation with thermodynamic properties such as K_{OW} , fugacity capacity in octanol, subcooled liquid vapor pressure, or the bioconcentration factor estimated in OPERA (Fig. S13).

Application of dosimetry model to exposure data

The model was applied to concentration-response data reported by Geier et al. (2018b) concerning nominal waterborne exposures of individual components of SM10 to dechorionated zebrafish from 6 to 120 hpf (Geier et al. 2018b). Dose-response curves were fit to the percent of malformed embryos to derive nominal BMD20 media concentrations (Fig. 8A). BMD20 refers to the amount of a chemical causing a 20% increase in a toxic outcome from control data. The AUC ($\mu\text{M} \times \text{h}$) tissue dose was calculated

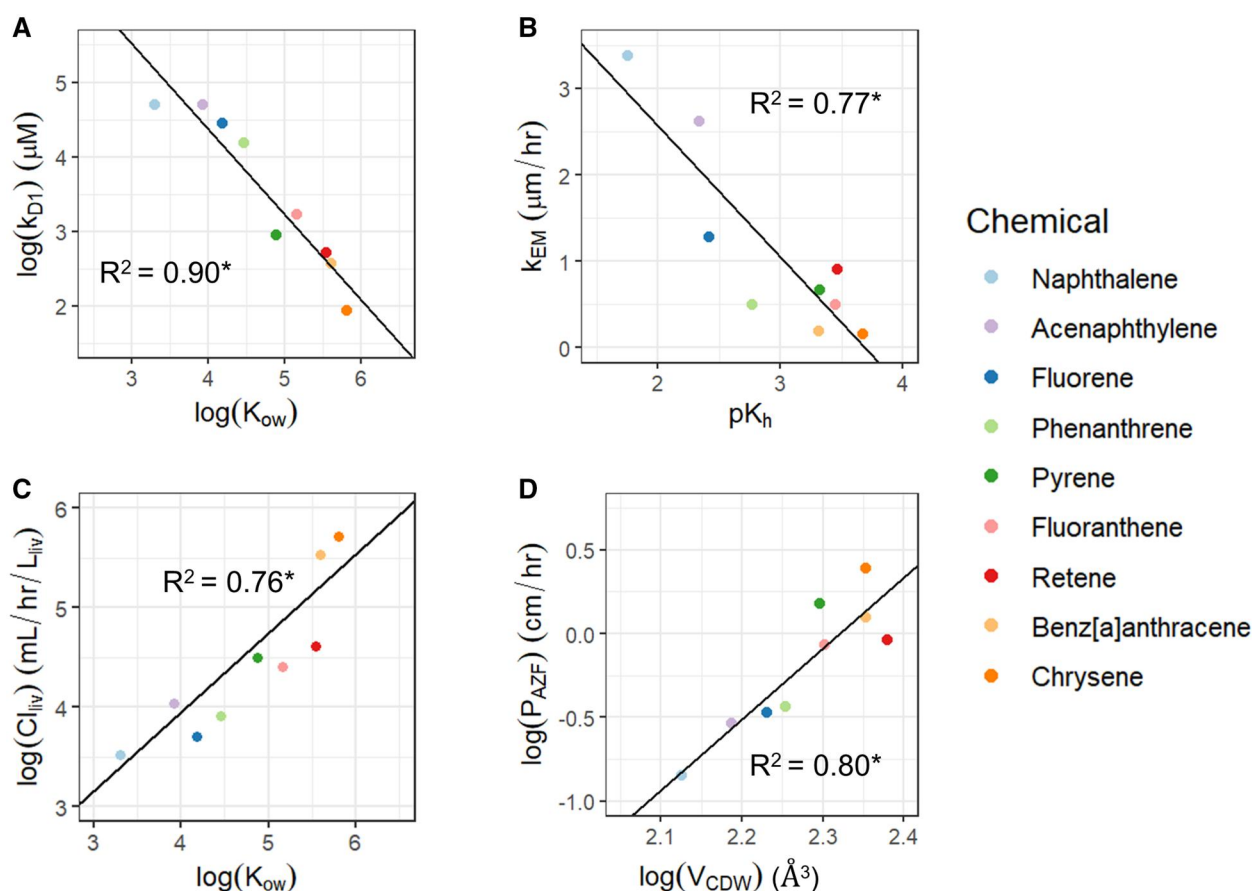


Fig. 7. Linear and log-linear models for: A) binding affinity (K_{D1}) and octanol–water partitioning coefficient (K_{OW}), B) the rate constant of elimination from the media (k_{EM}) and Henry's law (K_H), C) clearance from the liver (Cl_{LIV}) and K_{OW} , and D) the permeability of zebrafish to the compound (P_{AZF}) and Van Der Wall's volume (V_{VDW}). Models were fit in R. Asterisks (*) indicate P-values ≤ 0.05 for linear model.

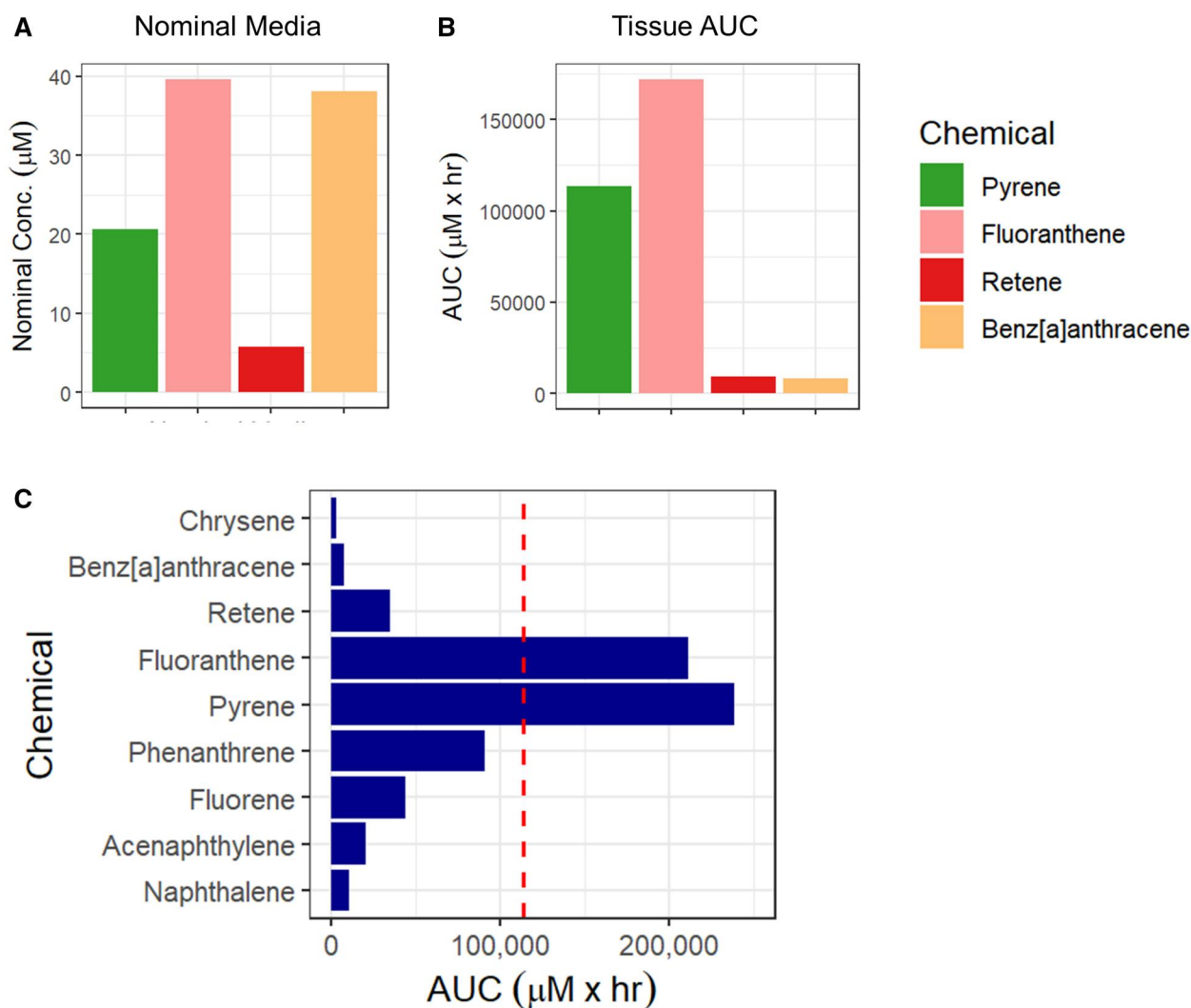


Fig. 8. Comparison of dose metrics for BMD20s for pyrene, fluoranthene, retene, and benz[a]anthracene in static waterborne exposures of dechlorinated zebrafish embryos. A) Nominal concentration is the amount of chemical added to the well divided by the volume of media. B) AUC is the area under the curve of the tissue concentration for the 6 to 120 hpf exposure as estimated by the dosimetry model. C) Comparison of the AUC of each chemical at 50 µM nominal exposures as predicted by the dosimetry model. Fifty micromolar was the maximum tested concentration for each chemical in Geier et al. (2018). The dashed red line indicates the AUC given by pyrene exposed at its nominal BMD20 (20.6 µM).

for each of the chemicals eliciting a BMD20 (Fig. 8B). Interpreted blindly, nominal exposure concentrations indicate that pyrene is more toxic than benz [a]anthracene; however, utilizing the AUC tissue dose, benz[a]anthracene causes toxicity in fish at a dose ~20× smaller than pyrene. Lastly, we predicted the AUC for all chemicals at nominal exposures of 50 µM, the maximum tested concentration in Geier et al. (Fig. 8C). The dashed red line indicates the AUC tissue dose for pyrene at its BMD20. Although retene and benz[a]anthracene were able to achieve toxicity at much lower AUCs than pyrene, it is not clear if the lack of observed toxicity for other compounds in SM10 is due to a true lack of toxicity or a lack of bioavailability. This is particularly true for compounds such as chrysene and naphthalene, which achieved modeled AUCs ~60 and 16 times less than that of pyrene at its BMD20.

Discussion

Developmental zebrafish assays have been used to generate toxicity data in an integrated vertebrate model for hundreds of

PAHs. Many of these studies report nominal exposure concentrations which has hampered comparison between chemicals and exposure systems. An end goal of our group is a biologically based kinetic dosimetry model, generalized for PAHs using intrinsic chemical properties, for accurate prediction of PAH dose in zebrafish embryos throughout developmental exposures. The model presented in this paper represents a significant step toward the realization of a generalized PAH model. It adequately describes volatile loss and plate wall binding with parameters that logically scale with expected thermodynamic properties. Moving forward, however, a generalized PAH model will require refinement in our understanding of mixture effects, clearance rates, partitioning between the zebrafish and media, and chemical-specific permeability.

Training the PAH model using mixture exposures had the advantage of parameterizing multiple chemicals within one experiment and revealed potential mixture effects for a subset of chemicals. Utilizing mixture exposures reduced the required sample prep, analytical time, and number of sacrificed zebrafish embryos while still parameterizing an effective model. The PAH

model predicted 48 hpf body burdens resulting from similar mixture exposures in a different study within a factor of 2 for 83% (20/24) of measurements and within a factor of 5 for 92% (22/24) of measurements. Performance diminished some for 48 hpf body burdens resulting from individual chemical exposures, predicting only 54% (13/24) of measurements within a factor of 2 and 87% (21/24) of measurements within a factor of 5. The increase in error for predictions of individual chemical exposures was likely partially caused by exposures being performed well above PAH solubility limits. Estimates for benz[a]anthracene and chrysene in individual PAH exposures accounted for all body burden estimations not within a factor of 5. In comparison, there is a clear decrease in the ratio of tissue burden to exposure concentration between individual exposures and mixture exposures for these compounds (Fig. S8). The noted shift between exposure types may result from mixture effects on xenobiotic metabolism. PAHs can inhibit each other's biotransformation by competing for active sites in metabolizing enzymes or by non-competitive inhibition (Willett et al. 1998, 2001; Smith et al. 2022). Both would result in underestimated clearance values from mixture exposures leading to overestimated tissue burdens in exposures to individual PAHs. Experiments investigating the rates of clearance in embryonic zebrafish for chemicals in individual and mixture exposures in sealed systems such as closed vial exposures could be used to determine the impact of competition for active sites in developmental exposures.

Early biotransformation of xenobiotics by zebrafish embryos is commonly described by first-order kinetics, however, most studies have not linked metabolic capacity to specific processes in development (Kühnert et al. 2013; Brox et al. 2016; Chelcea et al. 2023). The pseudo equilibrium model described in Simeon et al., and models based on it thereafter, have linked metabolic capacity to liver volume. They modeled liver growth utilizing the fractional liver volume in adult zebrafish fish and a liver growth onset time (Siméon et al. 2020; Billat et al. 2023a). We also scale clearance to liver growth in our model, but find a loglogistic model more suitable for describing liver growth in developing zebrafish (Fig. S1C). Both approaches set up a direct ontological link between liver volume and xenobiotic clearance in developing zebrafish. Conceptually, this is reasonable if the majority of metabolizing enzymes are present in the liver, or if the amount of metabolizing enzymes in the zebrafish remains roughly proportional to the liver size throughout development. For Ahr2 interacting compounds, including some PAHs, biotransformation has been demonstrated earlier in development than liver outgrowth, suggesting extrahepatic metabolism may be an important driver of PAH disposition in development (Sadler et al. 2007; Chu and Sadler 2009; Kühnert et al. 2013; Bräunig et al. 2015; Rude et al. 2024). Because of this, we tested if early extrahepatic biotransformation could be better accounted for by fitting clearance with a scalar that increased over an earlier time course than liver growth. Models with earlier metabolic growth times resulted in comparable fits to the original model scaling clearance directly with liver growth (Fig. 6). This suggests that approximating clearance in developing zebrafish by scaling to liver volume is functionally sufficient, if not entirely physiologically accurate. Further support for this method can be gained by comparing the fitted clearance values in this study to clearances measured in perfused rainbow trout livers and killifish S9 (Nichols et al. 2013; Fay et al. 2017; Franco et al. 2022). The rank order of fitted or measured clearance values for PAHs shared

between our study and Nichols et al. (2013) are identical: Pyrene>phenanthrene>fluorene>naphthalene (Fig. S14A). Additionally, with the exception of fluoranthene and pyrene, which have very close intrinsic clearances, the rank order of clearance values in the zebrafish dosimetry model and liver S9 from killifish are also conserved (Fig. S14B). It appears then that intrinsic clearance in future models could be informed by in vitro-measured clearances. Additionally, ab initio clearance values in future models may be predicted by quantitative structure–activity relationships relating in vitro or in vivo clearances to parameters measured in in silico docking studies of PAHs in the active sites of cytochrome P450s (Chen et al. 2021).

Zebrafish-media partitioning coefficients and chemical-specific permeability represent areas for model improvement in future iterations. Permeability was positively correlated with measurements of molecular size (Fig. 7D, Fig. S13) which is opposite to both theoretically expected and previously determined experimental trends (Kühnert et al. 2013; Miyamoto and Shimono 2020). Zebrafish media partitioning coefficients did not correlate strongly with any of the tested physchem properties (Fig. S14). The lack of expected behaviors for these 2 parameters may be due to incorrect assumptions about the bioavailability of undissolved compounds. In keeping with common practice, the presented model assumes that only freely dissolved chemical is bioavailable to the embryo (Dahan and Miller 2012; Lydy et al. 2014); however, it is not difficult to imagine precipitated chemical coming into contact with a zebrafish embryo in the confines of a 96-well plate thereby facilitating direct dermal absorption and inflating permeability estimations. Alternatively, the unexpected trends may arise from our experimental setup. To maximize applicability, our measurements were conducted in 96-well polystyrene plates which are imperfectly sealed, use small media volumes, and feature significant PAH binding to vessel walls. These conditions, along with limited early measurements, made for difficult parameter estimates. For better experimental measurements of zebrafish—media partitioning and permeability, future experiments would be served to obtain measurements under less dynamic conditions. As an example, Kühnert et al. (2013) obtained good results by conducting measurements of PAH in media and zebrafish embryos within sealed glass vials at concentrations well under the limit of solubility for test compounds.

An alternative approach could lean more heavily on ab initio estimation of permeability or zebrafish—media partitioning coefficients. For instance, the embryo could be described as mass fractions of storage lipid, phospholipid, protein, and water. Estimated or empirically derived partitioning coefficients into the above-named compartments could then be used to estimate zebrafish—media partition coefficients (Endo et al. 2013; Fischer et al. 2017; Fisher et al. 2019). The estimated zebrafish—media partitioning coefficients could then be used to constrain the model while fitting permeability to training data. Similarly, machine learning and quantitative structure—permeability relationship models have been developed to estimate permeability of compounds (Egan et al. 2000; Moss et al. 2002; Sharma et al. 2017; Sun et al. 2017). These could be adapted or applied to estimate the permeability in zebrafish to further constrain the model. We expect an approach utilizing ab initio estimations to selectively constrain some but not all parameters, may allow for faster development of intelligible, predictive models moving forward.

The single well-mixed compartment approximation of a zebrafish effectively modeled body burdens over time, providing a useful

and analytically verifiable dose metric with which to interpret PAH toxicities. Recent models have varied in approach; a few treating all organs as separate compartments (Siméon et al. 2020; Billat et al. 2023a, 2023b), some dividing the embryo into yolk and tissue compartments (Halbach et al. 2020; Chelcea et al. 2023), and still others utilizing a single compartment much like our own (Kühnert et al. 2013; Brox et al. 2016; Vogs et al. 2019; Warner et al. 2022). Complex models treating each organ as a separate compartment yield more specific dose metrics but make assumptions about the rate and extent of chemical transport within the developing fish that are not verifiable at this time. A middle path exists in treating the embryo as a yolk compartment and tissue compartment. This approach likely approximates separate tissue and yolk doses more accurately than a whole embryo body burden as at least 2 studies have shown significant preference of hydrophobic compounds to the yolk compartment (Halbach et al. 2020; Ulrich et al. 2020). Still analytical validation of separate yolk and tissue concentrations is much more challenging, and depending on study goals, not always necessary. Because we predicted whole-body burdens, analytical validation was straightforward via whole embryo extractions and GCMS/MS analysis. The single-compartment approach effectively modeled highly variable body burdens within developing embryos throughout exposure times. This dose metric allowed for the determination of integrated AUC doses to compare PAH potencies which showed that benz[a]anthracene and retene cause toxicity at much lower tissue doses than other constituents of SM10.

The PAH dose metrics estimated by this model will allow for greater interpretability of toxic outcomes in developmental zebrafish assays. Predicted tissue doses can be used to normalize data between different exposure scenarios such as flow-through versus static renewal exposures or 96-well plate versus sealed vial exposures. Zebrafish embryo dose metrics such as the AUC concentration or maximum tissue concentration will allow for comparison to other biological systems. We could for instance compare the AUC tissue dose of retene causing toxicity in a developing zebrafish to a modeled AUC cellular dose causing toxicity in a lung epithelial culture to an AUC tissue dose expected in human lung alveoli exposed to severe wildfire smoke or heavily polluted urban air. Such comparisons will help us understand which PAHs or mixtures of PAHs drive toxic outcomes and better prioritize future research directions.

Conclusion

This study presents a new biologically based toxicokinetic dosimetry model for waterborne exposures of developing zebrafish to PAHs. It demonstrates the utility and limitations of utilizing mixture experiments to parameterize for multiple chemicals within an individual experiment and clarifies exposure kinetics of 9 PAHs having K_H and K_{OW} spanning 3 orders of magnitude. Armed with this knowledge, it is clear that volatile loss, solubility, and binding to plastic plate walls have considerable influence on the dosimetry of PAHs. High losses noted for phenanthrene, fluorene, and naphthalene, indicate that volatile PAHs will require alternative means of exposure such as passive dosing or tightly sealed vial exposures in order to accurately access toxicity. We expect that a predictive generalized PAH dosimetry model accounting for zebrafish physiology and a variety of exposure scenarios will be possible with further investigation into the physchem properties governing PAH permeability, tissue—media partitioning, and clearance rates. As developmental zebrafish exposures are increasingly utilized for toxicological investigation, modeling such as this will increase interpretability of potency between

different compounds, comparison between different exposure methods, and translatability to inform both human health and environmental decision-making.

Acknowledgments

We are thankful for the zebrafish rearing and developmental screening teams at the Sinnhuber Aquatic Research Lab for providing zebrafish embryos as required. Thank you also to the Chemical Mixtures Core in the Oregon State University Superfund Research Center for providing SM10 and analytical chemistry measurements. We also thank Veronica Puig-Sanvicens at HP for technical help validating the bioprinter injections.

Supplementary material

Supplementary material is available at *Toxicological Sciences* online.

Funding

This research was supported by the National Institutes of Health (P42 ES016465, T32 ES007060, R35 ES031709, ES030287).

Conflicts of interest

None declared.

References

- Abdel-Shafy HI, Mansour MS. 2016. A review on polycyclic aromatic hydrocarbons: source, environmental impact, effect on human health and remediation. *Egypt J Pet*. 25:107–123.
- Akaike H. 1998. Information theory and an extension of the maximum likelihood principle. In: Parzen E, Tanabe K, Kitagawa G, editors. *Selected papers of Hirotugu Akaike*. New York (NY): Springer New York. p. 199–213.
- Allan SE, Sower GJ, Anderson KA. 2011. Estimating risk at a superfund site using passive sampling devices as biological surrogates in human health risk models. *Chemosphere*. 85:920–927.
- Al-Moubarak E, Shiels HA, Zhang Y, Du C, Hanington O, Harmer SC, Dempsey CE, Hancox JC. 2021. Inhibition of the hERG potassium channel by phenanthrene: a polycyclic aromatic hydrocarbon pollutant. *Cell Mol Life Sci*. 78:7899–7914.
- Anderson KA, Szelewski MJ, Wilson G, Quimby BD, Hoffman PD. 2015. Modified ion source triple quadrupole mass spectrometer gas chromatograph for polycyclic aromatic hydrocarbon analyses. *J Chromatogr A*. 1419:89–98.
- Arnot JA, Mackay D, Bonnell M. 2008. Estimating metabolic biotransformation rates in fish from laboratory data. *Environ Toxicol Chem*. 27:341–351.
- Beilmann M, Boonen H, Czich A, Dear G, Hewitt P, Mow T, Newham P, Oinonen T, Pognan F, Roth A, et al. 2019. Optimizing drug discovery by investigative toxicology: current and future trends. *Altex*. 36:289–313.
- Bell SM, Chang X, Wambaugh JF, Allen DG, Bartels M, Brouwer KLR, Casey WM, Choksi N, Ferguson SS, Fraczekiewicz G, et al. 2018. In vitro to in vivo extrapolation for high throughput prioritization and decision making. *Toxicol In Vitro*. 47:213–227.
- Billat PA, Brochot C, Brion F, Beaudouin R. 2023a. A PBPK model to evaluate zebrafish eleutheroembryos' actual exposure:

- bisphenol A and analogs' (AF, F, and S) case studies. *Environ Sci Pollut Res Int.* 30:7640–7653.
- Billat PA, Vogs C, Blassiau C, Brochot C, Wincent E, Brion F, Beaudouin R. 2023b. PBTK modeled perfluoroalkyl acid kinetics in zebrafish eleutheroembryos suggests impacts on bioconcentrations by chorion porosity dynamics. *Toxicol In Vitro.* 89:105588.
- Birch H, Kramer NI, Mayer P. 2019. Time-resolved freely dissolved concentrations of semivolatile and hydrophobic test chemicals in in vitro assays-measuring high losses and crossover by head-space solid-phase microextraction. *Chem Res Toxicol.* 32:1780–1790.
- Bräunig J, Schiwy S, Broedel O, Müller Y, Frohme M, Hollert H, Keiter SH. 2015. Time-dependent expression and activity of cytochrome P450 1s in early life-stages of the zebrafish (*Danio rerio*). *Environ Sci Pollut Res Int.* 22:16319–16328.
- Brette F, Shiels HA, Galli GLJ, Cros C, Incardona JP, Scholz NL, Block BA. 2017. A novel cardiotoxic mechanism for a pervasive global pollutant. *Sci Rep.* 7:41476.
- Brox S, Seiwert B, Kuster E, Reemtsma T. 2016. Toxicokinetics of polar chemicals in zebrafish embryo (*Danio rerio*): influence of physicochemical properties and of biological processes. *Environ Sci Technol.* 50:10264–10272.
- Byrd RH, Lu P, Nocedal J, Zhu C. 1995. A limited memory algorithm for bound constrained optimization. *SIAM J Sci Comput.* 16:1190–1208.
- Chelcea I, Vogs C, Hamers T, Koekkoek J, Legradi J, Sapounidou M, Örn S, Andersson PL. 2023. Physiology-informed toxicokinetic model for the zebrafish embryo test developed for bisphenols. *Chemosphere.* 345:140399.
- Chen C, Shen J, Yang L, Zhang W, Xia R, Huan F, Gong X, Wang L, Wang C, Yuan H, et al. 2021. Identification of structural properties influencing the metabolism of polycyclic aromatic hydrocarbons by cytochrome P450 1A1. *Sci Total Environ.* 758:143997.
- Chepelev NL, Moffat ID, Bowers WJ, Yauk CL. 2015. Neurotoxicity may be an overlooked consequence of benzo[a]pyrene exposure that is relevant to human health risk assessment. *Mutat Res Rev Mutat Res.* 764:64–89.
- Chlebowski AC, Tanguay RL, Simonich SL. 2016. Quantitation and prediction of sorptive losses during toxicity testing of polycyclic aromatic hydrocarbon (PAH) and nitrated PAH (NPAH) using polystyrene 96-well plates. *Neurotoxicol Teratol.* 57:30–38.
- Chu J, Sadler KC. 2009. New school in liver development: lessons from zebrafish. *Hepatology.* 50:1656–1663.
- Dahan A, Miller JM. 2012. The solubility-permeability interplay and its implications in formulation design and development for poorly soluble drugs. *AAPS J.* 14:244–251.
- Daley MC, Mende U, Choi BR, McMullen PD, Coulombe KLK. 2023. Beyond pharmaceuticals: fit-for-purpose new approach methodologies for environmental cardiotoxicity testing. *Altex.* 40:103–116.
- Egan WJ, Merz KM Jr, Baldwin JJ. 2000. Prediction of drug absorption using multivariate statistics. *J Med Chem.* 43:3867–3877.
- Endo S, Brown TN, Goss KU. 2013. General model for estimating partition coefficients to organisms and their tissues using the biological compositions and polyparameter linear free energy relationships. *Environ Sci Technol.* 47:6630–6639.
- Fang J, Dong S, Boogaard PJ, Rietjens I, Kamelia L. 2022. Developmental toxicity testing of unsubstituted and methylated 4- and 5-ring polycyclic aromatic hydrocarbons using the zebrafish embryotoxicity test. *Toxicol In Vitro.* 80:105312.
- Fay KA, Fitzsimmons PN, Hoffman AD, Nichols JW. 2017. Comparison of trout hepatocytes and liver S9 fractions as in vitro models for predicting hepatic clearance in fish. *Environ Toxicol Chem.* 36:463–471.
- Fischer FC, Cirpka OA, Goss KU, Henneberger L, Escher BI. 2018. Application of experimental polystyrene partition constants and diffusion coefficients to predict the sorption of neutral organic chemicals to multiwell plates in in vivo and in vitro bioassays. *Environ Sci Technol.* 52:13511–13522.
- Fischer FC, Henneberger L, König M, Bittermann K, Linden L, Goss KU, Escher BI. 2017. Modeling exposure in the TOX21 in vitro bioassays. *Chem Res Toxicol.* 30:1197–1208.
- Fisher C, Siméon S, Jamei M, Gardner I, Bois YF. 2019. VIVD: virtual in vitro distribution model for the mechanistic prediction of intracellular concentrations of chemicals in in vitro toxicity assays. *Toxicol In Vitro.* 58:42–50.
- Franco ME, Johanning K, Matson CW, Lavado R. 2022. Reduced biotransformation of polycyclic aromatic hydrocarbons (PAHs) in pollution-adapted Gulf killifish (*Fundulus grandis*). *Sci Total Environ.* 806:150854.
- Garcia GR, Noyes PD, Tanguay RL. 2016. Advancements in zebrafish applications for 21st century toxicology. *Pharmacol Ther.* 161:11–21.
- Garland MA, Geier MC, Bugel SM, Shankar P, Dunham CL, Brown JM, Tilton SC, Tanguay RL. 2020. Aryl hydrocarbon receptor mediates larval zebrafish fin duplication following exposure to benzofluoranthenes. *Toxicol Sci.* 176:46–64.
- Geier MC, Chlebowski AC, Truong L, Massey Simonich SL, Anderson KA, Tanguay RL. 2018a. Comparative developmental toxicity of a comprehensive suite of polycyclic aromatic hydrocarbons. *Arch Toxicol.* 92:571–586.
- Geier MC, James Minick D, Truong L, Tilton S, Pande P, Anderson KA, Teeguarden J, Tanguay RL. 2018b. Systematic developmental neurotoxicity assessment of a representative PAH superfund mixture using zebrafish. *Toxicol Appl Pharmacol.* 354:115–125.
- Genter MB, Marlowe J, Kevin Kerzee J, Dragin N, Puga A, Dalton TP, Nebert DW. 2006. Naphthalene toxicity in mice and aryl hydrocarbon receptor-mediated CYPs. *Biochem Biophys Res Commun.* 348:120–123.
- Goodale BC, Tilton SC, Corvi MM, Wilson GR, Janszen DB, Anderson KA, Waters KM, Tanguay RL. 2013. Structurally distinct polycyclic aromatic hydrocarbons induce differential transcriptional responses in developing zebrafish. *Toxicol Appl Pharmacol.* 272:656–670.
- Guo Y, Veneman WJ, Spaink HP, Verbeek FJ. 2017. Three-dimensional reconstruction and measurements of zebrafish larvae from high-throughput axial-view in vivo imaging. *Biomed Opt Express.* 8:2611–2634.
- Halbach K, Ulrich N, Goss KU, Seiwert B, Wagner S, Scholz S, Luckenbach T, Bauer C, Schweiger N, Reemtsma T. 2020. Yolk sac of zebrafish embryos as backpack for chemicals? *Environ Sci Technol.* 54:10159–10169.
- Her GM, Chiang CC, Chen WY, Wu JL. 2003. In vivo studies of liver-type fatty acid binding protein (L-FABP) gene expression in liver of transgenic zebrafish (*Danio rerio*). *FEBS Lett.* 538:125–133.
- Hill AJ, Teraoka H, Heideman W, Peterson RE. 2005. Zebrafish as a model vertebrate for investigating chemical toxicity. *Toxicol Sci.* 86:6–19.
- Howe K, Clark MD, Torroja CF, Torrance J, Berthelot C, Muffato M, Collins JE, Humphray S, McLaren K, Matthews L, et al. 2013. The zebrafish reference genome sequence and its relationship to the human genome. *Nature.* 496:498–503.
- Incardona JP, Day HL, Collier TK, Scholz NL. 2006. Developmental toxicity of 4-ring polycyclic aromatic hydrocarbons in zebrafish is differentially dependent on AH receptor isoforms and hepatic

- cytochrome P4501A metabolism. *Toxicol Appl Pharmacol*. 217:308–321.
- Incardona JP, Linbo TL, Cameron JR, Scholz NL. 2024. Structure-activity relationships for alkyl-phenanthrenes support two independent but interacting synergistic models for PAC mixture potency. *Sci Total Environ*. 918:170544.
- Jarema KA, Hunter DL, Hill BN, Olin JK, Britton KN, Waalkes MR, Padilla S. 2022. Developmental neurotoxicity and behavioral screening in larval zebrafish with a comparison to other published results. *Toxics*. 10:256.
- Juberg DR, Fox DA, Forcelli PA, Kacew S, Lipscomb JC, Saghir SA, Sherwin CM, Koenig CM, Hays SM, Kirman CR. 2023. A perspective on in vitro developmental neurotoxicity test assay results: an expert panel review. *Regul Toxicol Pharmacol*. 143:105444.
- Kimmel CB, Ballard WW, Kimmel SR, Ullmann B, Schilling TF. 1995. Stages of embryonic development of the zebrafish. *Dev Dyn*. 203:253–310.
- Knecht AL, Goodale BC, Truong L, Simonich MT, Swanson AJ, Matzke MM, Anderson KA, Waters KM, Tanguay RL. 2013. Comparative developmental toxicity of environmentally relevant oxygenated PAHs. *Toxicol Appl Pharmacol*. 271:266–275.
- Kramer NI, Krismartina M, Rico-Rico A, Blaauboer BJ, Hermens JL. 2012. Quantifying processes determining the free concentration of phenanthrene in basal cytotoxicity assays. *Chem Res Toxicol*. 25:436–445.
- Kühnert A, Vogs C, Altenburger R, Küster E. 2013. The internal concentration of organic substances in fish embryos—a toxicokinetic approach. *Environ Toxicol Chem*. 32:1819–1827.
- Kuhnert A, Vogs C, Seiwert B, Aulhorn S, Altenburger R, Hollert H, Kuster E, Busch W. 2017. Biotransformation in the zebrafish embryo-temporal gene transcription changes of cytochrome P450 enzymes and internal exposure dynamics of the AhR binding xenobiotic benz[a]anthracene. *Environ Pollut*. 230:1–11.
- Kwon HC, Kwon JH. 2012. Measuring aqueous solubility in the presence of small cosolvent volume fractions by passive dosing. *Environ Sci Technol*. 46:12550–12556.
- Lindberg CD, Di Giulio RT. 2019. Polycyclic aromatic hydrocarbon and hypoxia exposures result in mitochondrial dysfunction in zebrafish. *Aquat Toxicol*. 216:105298.
- Lydy MJ, Landrum PF, Oen AM, Allinson M, Smedes F, Harwood AD, Li H, Maruya KA, Liu J. 2014. Passive sampling methods for contaminated sediments: state of the science for organic contaminants. *Integr Environ Assess Manag*. 10:167–178.
- MacArthur Clark J. 2018. The 3Rs in research: a contemporary approach to replacement, reduction and refinement. *Br J Nutr*. 120:S1–S7.
- MacRae CA, Peterson RT. 2015. Zebrafish as tools for drug discovery. *Nat Rev Drug Discov*. 14:721–731.
- Magnolia Sciences. RMagnolia: run Magnolia models within R. V 1.3.15 Orlando (FL): Magnolia Sciences LLC. <https://www.magnoliasci.com/>
- Mandrell D, Truong L, Jephson C, Sarker MR, Moore A, Lang C, Simonich MT, Tanguay RL. 2012. Automated zebrafish chorion removal and single embryo placement: optimizing throughput of zebrafish developmental toxicity screens. *J Lab Autom*. 17:66–74.
- Mansouri K, Grulke CM, Judson RS, Williams AJ. 2018. Opera models for predicting physicochemical properties and environmental fate endpoints. *J Cheminform*. 10:10.
- Marques M, Mari M, Audi-Miro C, Sierra J, Soler A, Nadal M, Domingo JL. 2016. Photodegradation of polycyclic aromatic hydrocarbons in soils under a climate change base scenario. *Chemosphere*. 148:495–503.
- Minick DJ, Anderson KA. 2017. Diffusive flux of PAHs across sediment-water and water-air interfaces at urban superfund sites. *Environ Toxicol Chem*. 36:2281–2289.
- Miyamoto S, Shimono K. 2020. Molecular modeling to estimate the diffusion coefficients of drugs and other small molecules. *Molecules*. 25:5340.
- Morshead ML, Truong L, Simonich MT, Moran JE, Anderson KA, Tanguay RL. 2025. Developmental toxicity of alkylated PAHs and substituted phenanthrenes: structural nuances drive diverse toxicity and AHR activation. *Chemosphere*. 370:143894.
- Moss GP, Dearden JC, Patel H, Cronin MT. 2002. Quantitative structure-permeability relationships (QSPRs) for percutaneous absorption. *Toxicol In Vitro*. 16:299–317.
- Nawaji T, Yamashita N, Umeda H, Zhang S, Mizoguchi N, Seki M, Kitazawa T, Teraoka H. 2020. Cytochrome P450 expression and chemical metabolic activity before full liver development in zebrafish. *Pharmaceuticals (Basel)*. 13:456.
- Nichols JW, Hoffman AD, ter Laak TL, Fitzsimmons PN. 2013. Hepatic clearance of 6 polycyclic aromatic hydrocarbons by isolated perfused trout livers: prediction from in vitro clearance by liver S9 fractions. *Toxicol Sci*. 136:359–372.
- Nichols JW, Ladd MA, Fitzsimmons PN. 2018. Measurement of kinetic parameters for biotransformation of polycyclic aromatic hydrocarbons by trout liver S9 fractions: implications for bioaccumulation assessment. *Appl In Vitro Toxicol*. 4:365–378.
- Padilla S, Corum D, Padnos B, Hunter DL, Beam A, Houck KA, Sipes N, Kleinstreuer N, Knudsen T, Dix DJ, et al. 2012. Zebrafish developmental screening of the ToxCast phase I chemical library. *Reprod Toxicol*. 33:174–187.
- Paul Friedman K, Gagne M, Loo LH, Karamertzanis P, Netzeva T, Sobanski T, Franzosa JA, Richard AM, Lougee RR, Gissi A, et al. 2020. Utility of in vitro bioactivity as a lower bound estimate of in vivo adverse effect levels and in risk-based prioritization. *Toxicol Sci*. 173:202–225.
- R Core Team. 2023. R: a language and environment for statistical computing. Vienna (Austria): R Foundation for Statistical Computing. <https://www.R-project.org/>.
- R Core Team. 2024. RStudio: integrated development environment for R. 2023.12.1.402. Vienna (Austria): Foundation for Statistical Computing. <https://www.r-project.org/>
- Ravindra K, Sokhi R, Van Grieken R. 2008. Atmospheric polycyclic aromatic hydrocarbons: source attribution, emission factors and regulation. *Atmos Environ*. 42:2895–2921.
- RDKit Team. 2023. RDKit: open-source cheminformatics software. V 2024.09.06. [accessed 2024 Dec 10]. <https://www.rdkit.org/>
- Ritz C, Baty F, Streibig JC, Gerhard D. 2015. Dose-response analysis using R. *PLoS One*. 10:e0146021.
- Rude CI, Wilson LB, La Du J, Lalli PM, Colby SM, Schultz KJ, Smith JN, Waters KM, Tanguay RL. 2024. Aryl hydrocarbon receptor-dependent toxicity by retene requires metabolic competence. *Toxicol Sci*. 202:50–68.
- Sadler KC, Krahn KN, Gaur NA, Ukomadu C. 2007. Liver growth in the embryo and during liver regeneration in zebrafish requires the cell cycle regulator, uhrf1. *Proc Natl Acad Sci USA*. 104:1570–1575.
- Schreiber R, Altenburger R, Paschke A, Kuster E. 2008. How to deal with lipophilic and volatile organic substances in microtiter plate assays. *Environ Toxicol Chem*. 27:1676–1682.
- Shankar P, Geier MC, Truong L, McClure RS, Pande P, Waters KM, Tanguay RL. 2019. Coupling genome-wide transcriptomics and developmental toxicity profiles in zebrafish to characterize polycyclic aromatic hydrocarbon (PAH) hazard. *Int J Mol Sci*. 20:2570.

- Sharma AK, Srivastava GN, Roy A, Sharma VK. 2017. ToxiM: a toxicity prediction tool for small molecules developed using machine learning and chemoinformatics approaches. *Front Pharmacol*. 8:880.
- Shultz MA, Choudary PV, Buckpitt AR. 1999. Role of murine cytochrome P-450 2F2 in metabolic activation of naphthalene and metabolism of other xenobiotics. *J Pharmacol Exp Ther*. 290:281–288.
- Siddens LK, Larkin A, Krueger SK, Bradfield CA, Waters KM, Tilton SC, Pereira CB, Löhr CV, Arlt VM, Phillips DH, et al. 2012. Polycyclic aromatic hydrocarbons as skin carcinogens: comparison of benzo[a]pyrene, dibenzo[def, p]chrysene and three environmental mixtures in the FVB/N mouse. *Toxicol Appl Pharmacol*. 264:377–386.
- Siméon S, Brotzmann K, Fisher C, Gardner I, Silvester S, MacLennan R, Walker P, Braunbeck T, Bois FY. 2020. Development of a generic zebrafish embryo PBPK model and application to the developmental toxicity assessment of valproic acid analogs. *Reprod Toxicol*. 93:219–229.
- Smith JN, Gaither KA, Pande P. 2022. Competitive metabolism of polycyclic aromatic hydrocarbons (PAHs): an assessment using in vitro metabolism and physiologically based pharmacokinetic (PBPK) modeling. *Int J Environ Res Public Health*. 19:8266.
- Sun H, Nguyen K, Kerns E, Yan Z, Yu KR, Shah P, Jadhav A, Xu X. 2017. Highly predictive and interpretable models for pampa permeability. *Bioorg Med Chem*. 25:1266–1276.
- Thomas RS, Bahadori T, Buckley TJ, Cowden J, Deisenroth C, Dionisio KL, Frithsen JB, Grulke CM, Gwinn MR, Harrill JA, et al. 2019. The next generation blueprint of computational toxicology at the us environmental protection agency. *Toxicol Sci*. 169:317–332.
- Truong L, Rericha Y, Thunga P, Marvel S, Wallis D, Simonich MT, Field JA, Cao D, Reif DM, Tanguay RL. 2022. Systematic developmental toxicity assessment of a structurally diverse library of PFAS in zebrafish. *J Hazard Mater*. 431:128615.
- U.S. EPA. 2024. Estimation programs interface suite for Microsoft Windows. V 4.11. Washington (DC): United State Environmental Protection Agency. <https://www.epa.gov/tsca-screening-tools/download-epi-suite-estimation-program-interface-v411>
- Ulrich N, Schweiger N, Pfennigsdorff A, Scholz S, Goss KU. 2020. Yolk-water partitioning of neutral organic compounds in the model organism *Danio rerio*. *Environ Toxicol Chem*. 39:1506–1516.
- Vogs C, Johanson G, Näslund M, Wulff S, Sjödin M, Hellstrandh M, Lindberg J, Wincent E. 2019. Toxicokinetics of perfluorinated alkyl acids influences their toxic potency in the zebrafish embryo (*Danio rerio*). *Environ Sci Technol*. 53:3898–3907.
- Warner RM, Sweeney LM, Hayhurst BA, Mayo ML. 2022. Toxicokinetic modeling of per- and polyfluoroalkyl substance concentrations within developing zebrafish (*Danio rerio*) populations. *Environ Sci Technol*. 56:13189–13199.
- Weaver RJ, Valentin JP. 2019. Today's challenges to de-risk and predict drug safety in human “mind-the-gap”. *Toxicol Sci*. 167:307–321.
- Wickham H. 2016. Ggplot2: elegant graphics for data analysis. New York: Springer-Verlag. <https://ggplot2.tidyverse.org>.
- Willett KL, Randerath K, Zhou GD, Safe SH. 1998. Inhibition of CYP1A1-dependent activity by the polynuclear aromatic hydrocarbon (PAH) fluoranthene. *Biochem Pharmacol*. 55:831–839.
- Willett KL, Wassenberg D, Lienesch L, Reichert W, Di Giulio RT. 2001. In vivo and in vitro inhibition of CYP1A-dependent activity in *Fundulus heteroclitus* by the polynuclear aromatic hydrocarbon fluoranthene. *Toxicol Appl Pharmacol*. 177:264–271.
- Williams AJ, Grulke CM, Edwards J, McEachran AD, Mansouri K, Baker NC, Patlewicz G, Shah I, Wambaugh JF, Judson RS, et al. 2017. The CompTox Chemistry Dashboard: a community data resource for environmental chemistry. *J Cheminform*. 9:61.
- Yu P, Duan Z, Liu S, Pachon I, Ma J, Hemstreet GP, Zhang Y. 2021. Drug-induced nephrotoxicity assessment in 3D cellular models. *Micromachines (Basel)*. 13:3.